POST-STACK SEISMIC CHARACTERIZATION OF PORE STRUCTURE VARIATIONS FOR PREDICTING PERMEABILITY HETEROGENEITY IN DEEPLY-BURIED CARBONATE RESERVOIRS, PUGUANG GAS FIELD, CHINA

A Thesis

by

JINGYI GUO

Submitted to the Office of Graduate and Professional Studies of
Texas A&M University
in partial fulfillment of the requirements for the degree of

MASTER OF SCIENCE

Chair of Committee,	Yuefeng Sun
Committee Members,	Michael C. Pope
	Berna Hascakir
Head of Department,	Michael C. Pope

December 2018

Major Subject: Geology

ABSTRACT

Alteration of depositional environment and diagenesis of carbonate rocks create various pore structures that cause strong heterogeneity in permeability. In this research, the petrophysical and elastic characteristics of diverse carbonate reservoir pore types in deeply-buried Puguang Gas Field, China are analyzed by integrating core, well log and seismic data.

Core and well log measurements were first investigated using a frame flexibility factor (γ) derived from a rock physics model of poroelasticity to classify different pore types in Feixianguan Formation of Puguang Gas Field and build the relationship between porosity and permeability for different pore type groups. The frame flexibility factor (γ) has a good correlation with pore shape instead of porosity and can be used as the pore structure indicator to classify moldic ($\gamma < 4.5$), intercrystalline ($5.5 < \gamma < 15$), and microcrystalline pores ($\gamma > 15$) in the studied reservoir. When $4.5 < \gamma < 5.5$, the reservoir rocks have mixed pore types, including both moldic and intercrystalline pores. Two distinct permeability trends were observed within two main pore types. At a similar porosity value, permeability is high in well-connected intercrystalline pores and low in isolated moldic pores.

The effect of pore structure variations on acoustic velocity and impedance was then quantified using the pore structure indicator (γ). A more linear correlation of acoustic impedance (AI) and the product of porosity and γ was established. Results show that moldic pores have higher AI, whereas intercrystalline pores have lower AI at a given

porosity. These relationships were used to interpret seismic AI inversion results and estimate the spatial variation of permeability using the post-stack seismic data. Moldic pores generated in platform margin ooid shoals and restricted platform after exposure and selectively dissolution as well as refluxion have lower permeability appearing as high AI; whereas dolostone with intercrystalline pores deposited in platform margin experienced reflux and burial dolomitization has relatively higher permeability, manifested in low AI values. The result shows great influence of varied carbonate pore structures on permeability heterogeneity and can be useful for further reservoir properties prediction.

DEDICATION

To my parents Xusheng Guo and Hong Li for their encouragement and support during the whole study.

ACKNOWLEDGEMENTS

I would like to thank my committee chair, Dr. Yuefeng Sun for his guidance and concern in various aspects. And I want to thank my committee members, Dr. Pope and Dr. Hascakir for their guidance and help throughout my master research.

My grateful thanks go to my friends and colleagues and the department faculty and staff for all their support and making my time at Texas A&M University a great experience.

I also thank CGG Company for providing Hampson-Russell software package for my master research.

Finally, I really appreciate the encouragement and love from my family.

CONTRIBUTORS AND FUNDING SOURCES

This work was supervised by a thesis committee consisting of Dr. Yuefeng Sun [advisor] and Dr. Michael Pope of the Department of Geology and Geophysics and Dr. Berna Hascakir of the Department of Petroleum Engineering.

The data used in this study was provided by SINOPEC, China to support academic research of the Reservoir Geophysics Program in the Department of Geology and Geophysics, Texas A&M University.

All other work conducted for the thesis was completed by the student, under the advisement of Dr. Yuefeng Sun.

Graduate study was supported by a fellowship from Williford Scholarship.

NOMENCLATURE

AI	Acoustic Impedance
HST	High-stand System Tract
RMS	Root-mean-square
SB	Sequence Boundary
TST	Transgressive System Tract
ρ	Density
ϕ	Porosity
V_{p}	Compressional Wave Velocity
V_{s}	Shear Wave Velocity
K	Bulk Modulus
K_{d}	Dry Frame Bulk Modulus
K_{s}	Solid Bulk Modulus
μ	Shear Modulus
μ_{d}	Dry Frame Shear Modulus
μ_{s}	Solid Shear Modulus
γ	Frame Flexibility Factor
γ_{μ}	Shear Frame Flexibility Factor

TABLE OF CONTENTS

Page

LIST OF FIGURES

Page

CHAPTER I

INTRODUCTION

Carbonate rocks, with a proportion of 60% oil and 40% gas reserves around world, are important conventional hydrocarbon reservoirs. However, because of the heterogeneous reservoir quality in carbonate fields, the oil and gas recovery rate is much lower than that in sandstone fields (Zhang, 2014). Originated from calcareous organisms, most carbonate rocks have quite different rock textures than those in sandstone. For carbonate minerals, the sensitivity to chemical reaction during deposition and diagenetic processes gives rise to great difficulty in predicting pore structure, porosity and permeability. Diagenesis such as dolomitization and dissolution can be significant for improving porosity and permeability in carbonate rocks, while cementation and compaction will reduce pore and throat space, resulting in decreasing of porosity and permeability. Unique diagenetic processes lead to different pore structures; furthermore, distinct pore types play an important role in controlling various characteristics of rock properties. The analysis of carbonate pore structure characterization can not only help to get a better understanding of how depositional environment and diagenesis impact the development of diverse pore types, but also find carbonate reservoirs with higher permeability.

I.1 Research Background

It is important to effectively describe carbonate reservoir spatial distribution and predict reservoir performance for oil and gas exploration and exploitation in carbonate fields. However, the susceptibility of carbonate rocks to depositional environment and complicated diagenesis make it difficult to predict carbonate rock properties. Dolomitization is one of the major diagenetic factors for carbonate rock, which formed by several models and occurs in numerous different environments. Limestone transforms to dolostone within the appropriate conditions and experiences modifications after deep burial (Ma et al., 2007). The rock type and pore structure also change during these processes, which leads to the unpredictability for carbonate rock features. Even rocks with similar porosity may have permeability difference of several orders in magnitude. Therefore, an accurate method to quantify the influence of geological controls on variation of pore structure and permeability is needed to study carbonate reservoirs and predict reservoir quality.

In previous studies, Sun (2000) introduced a rock physics model, and defined elastic parameters, named frame flexibility factors, which can be used to indicate different pore structures. Huang (2015) used shear frame flexibility factor from Sun's carbonate rock physics model to classify carbonate pore types. Zhang (2014) presented the method to predict reservoir fluid saturation based on post-stack impedance inversion. Thus, after establishing the relationship between rock pore types and petrophysical parameters, expressed on seismic data, this study analyzes reservoir characterization developed in the

field to understand the effect of diverse pore structures on spatial permeability heterogeneity.

I.2 Research Objective

The goal of this research is to determine carbonate reservoir pore structure characterization and predict permeability heterogeneity through the integration of core, well log, and seismic data. Specifically, to determine the relationship between porosity and permeability for different pore structures using the frame flexibility factor and study reservoir permeability spatial distribution features by combining post-stack seismic inversion results with seismic interpretation. The first objective of this research is to quantify the characteristics of carbonate pore structure and permeability and interpret post-stack inversion using relations between petrophysical properties and acoustic impedance obtained from core and log analysis.

The primary objective of this research is to quantify the characteristics of carbonate pore structures and permeability and interpret post-stack inversion using relationships between petrophysical properties and acoustic impedance. Using the rock physics model, frame flexibility factor (γ, γ_μ) can be calculated from sonic, density and porosity log data along with percentage of mineral components and elastic parameters such as bulk modulus and shear modulus. These frame flexibility factors (γ, γ_μ) can be indicators of different pore structures which are observed from thin sections in the reservoir of the studied area. After crossplotting core porosity and core permeability quantified with frame flexibility factor (γ), the relationship between permeability and pore types can thus

be established. A well section containing pore structure, core porosity, and core permeability is completed to understand the relation between permeability and pore structure for the cored wells.

The post-stack inversion interpreted as acoustic impedance can be related to the product of porosity and the frame flexibility factor (γ). Besides, the core permeability is related to the product of porosity and frame flexibility factor (γ). Comparing the acoustic impedance inversion with well analysis results which consist of pore structure, frame flexibility factor (γ), core porosity, and core permeability provides a more detailed understanding of reservoir permeability heterogeneity for different pore structures, rather than just interpreting the acoustic impedance lithologically and structurally.

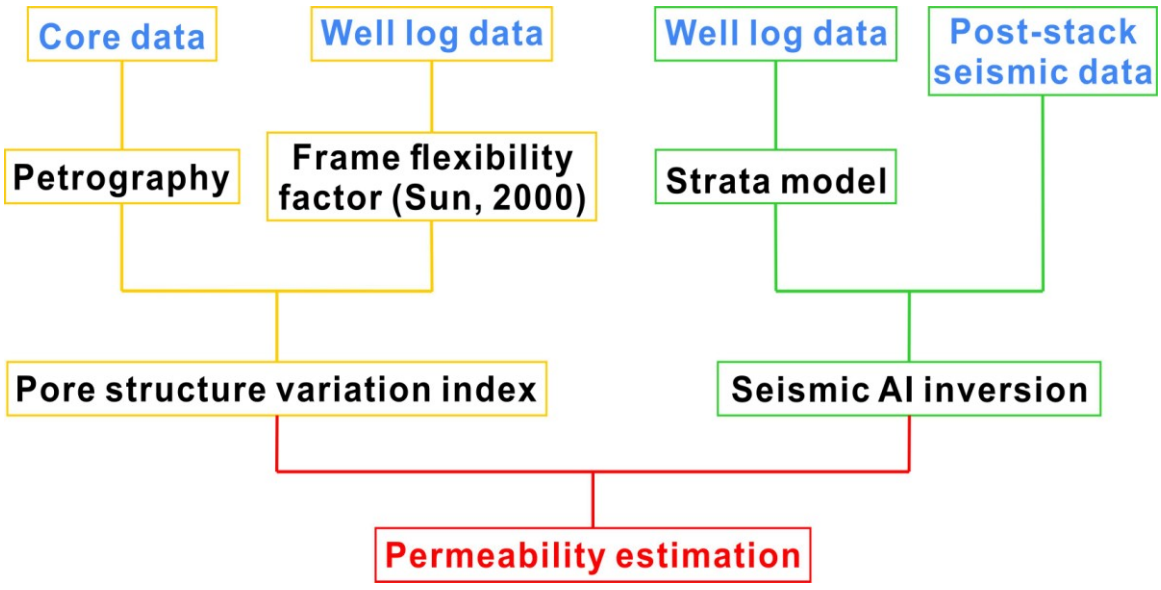

Figure 1.1: Summary of methodology and workflow applied for this study.

I.3 Datasets

The datasets used for this study are from a deeply-buried carbonate formation in Puguang Gas Field, Sichuan, China. The Permian-Triassic reservoirs from this studied area are located at a depth of about 5-6 km from the surface (Huang, 2015). In the studies area, well log data from 8 wells, such as gamma ray (GR), resistivity, sonic velocity, density, neutron-porosity, etc., were acquired. All of the 8 wells have shear wave velocity logs. Core measurements including pore porosity, pore permeability, and thin sections are available from 4 wells. The main studied wells, well A and well B, contain 655 core measurements of porosity and permeability and 55 thin sections; 617 core measurements of porosity and permeability and 266 thin sections, respectively. A seismic post-stack volume was provided. The relatively low resolution seismic dataset A contains 1109 inlines and 998 cross-lines, with a frequency range between 1 and 70 Hz.

CHAPTER II

GEOLOGICAL BACKGROUND

The studied dataset is from Puguang Gas Field (PGF) located in eastern Sichuan fold-thrust belt of the Sichuan Basin, southwest China (Figure 2.1A, C). This field was discovered in 2003, and has a proven gas volume of 350 × 109 m^3 (12.36TCFG) (Ma et al., 2007).

In Puguang gas field, the main source rocks consist of Lower Silurian and Upper Permian shales; Lower Triassic Feixianguan and Upper Permian Changxing Formations are reservoir rocks; and the thick anhydrite layers in the Jialingjiang and Leikoupo formations provide effective seal for gas accumulation. Due to deep burial, the hydrocarbon in the paleotrap was cracked into thermal gas (Cai et al., 2004). Most of the gas in the field is contained in the Feixianguan Formation, trapped in NNE-trending faulted anticlines, on the northern part of the structural belt. Sedimentary facies in this formation change upward from open platform, platform-margin ooid shoal, and restricted platform to evaporitic platform (Ma et al., 2007). The diagenesis, especially the dolomitization after deep burial, produced a complex pore structure system and increased the reservoir heterogeneity in the carbonate rocks, which leads to difficulty in predicting reservoir heterogeneity (Zhang et al., 2013).

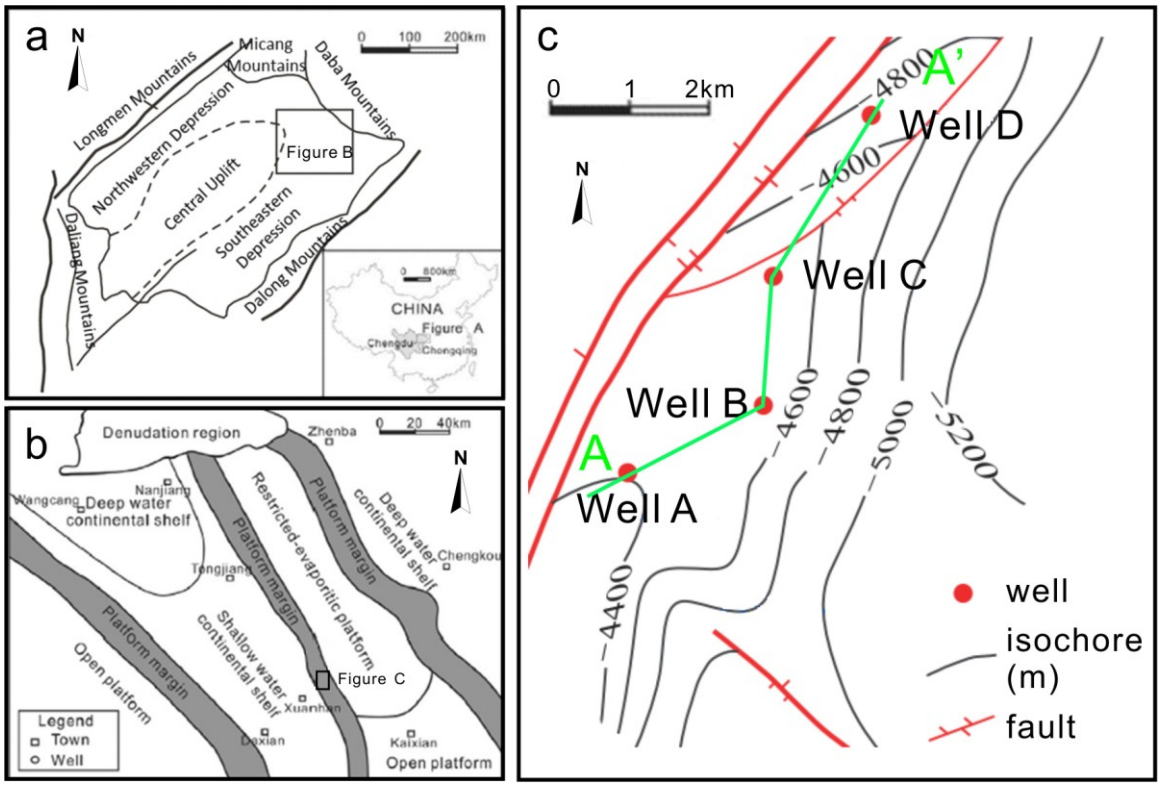

Figure 2.1: a) Topography and structure map of the Sichuan Basin and location of Puguang gas field in the eastern Sichuan fold belt. **b)** Paleogeography map of northeastern part of Sichuan Basin in Lower Triassic Feixianguan Formation and the location of the field. **c)** Structure map of Puguang Gas Field. The location of four main studied wells is shown. The "A-A' line shows the cross section of data in Chapter III and IV. (Modified from Sun et al., 2015 and Yu et al., 2015).

II.1 Tectonic Setting

The studied area is located in northeastern Sichuan Basin, southwest China, on the western part of the Yangtze craton and covers an area of 180,000 km^2 (Ma et al., 2007). The basin is structurally bounded by the Longmen Mountains in the northwest, the Micang Mountains in the north, the Daba Mountains in the northeast, the Dalou Mountains in the southeast, and the Daliang Mountains in the southwest (Figure 2.1A).

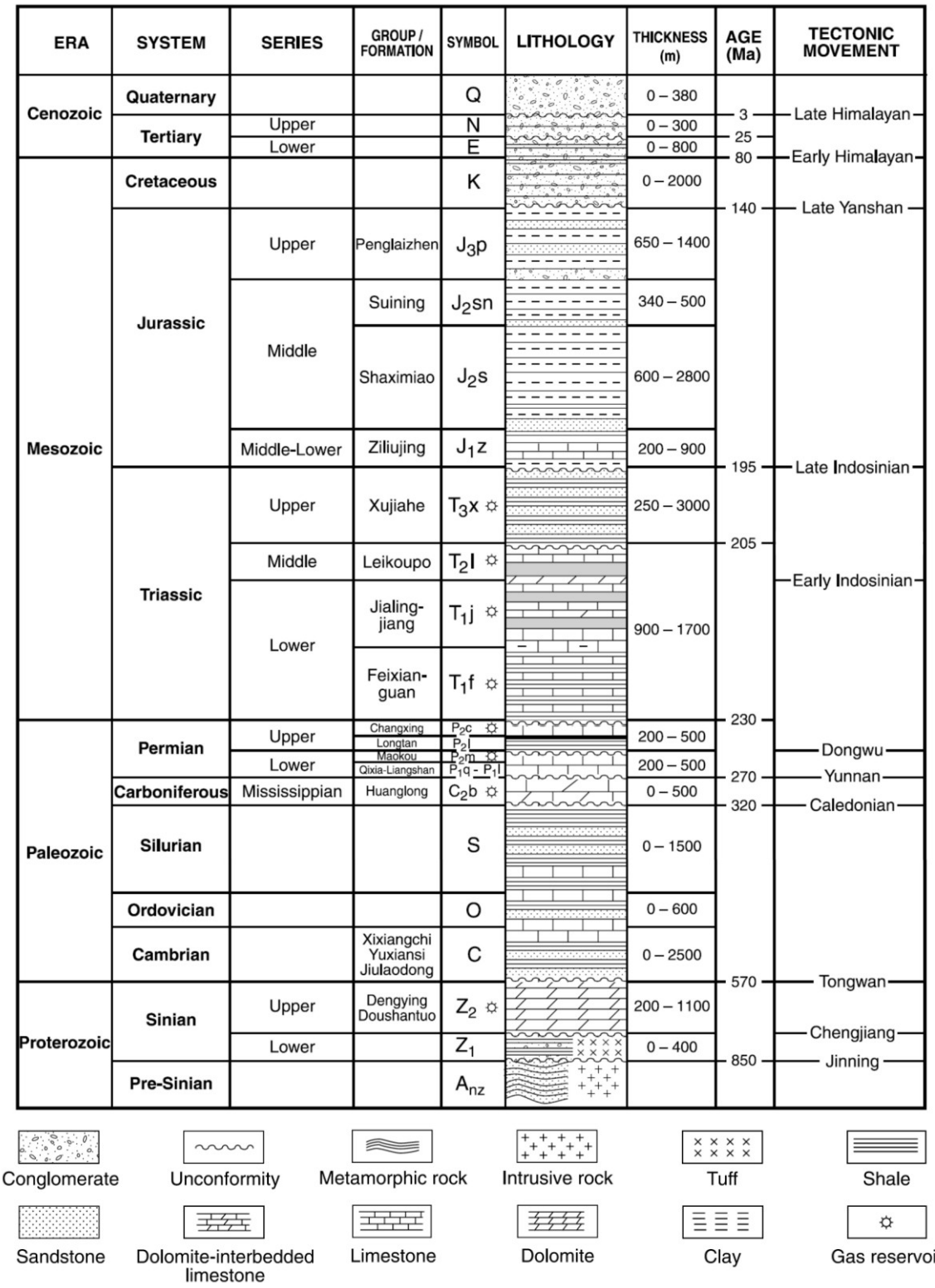

Figure 2.2: Generalized stratigraphy and tectonic history of the Sichuan Basin. (Modified from Ma et al., 2007).

From the Late Proterozoic to Triassic, Sichuan Basin was a passive margin in marine environment. Until Late Permian, this basin experienced four major marine transgressions, and each depositional succession consisted of sandstone, dolostone, limestone, and shale, above the basement of metamorphic rocks. With the Dongwu tectonic movement from Late Permian to Early Triassic, the fifth marine transgression led to the deposition of coal-bearing shale and shallow-marine carbonate (Cai et al., 2004; Ma et al., 2007) (Figure 2.2). Overlying the Longtan Formation, which is the source rock of the field, reefal dolomite skeletal wacke-packstone of the Upper Permian Changxing Formation and platform-margin shoal dolomite oolitic grainstone of the Lower Triassic Feixianguan Formation are the main component of northeastern Sichuan carbonate platform and provide the main reservoirs to the Puguang field and other fields in eastern Sichuan. From the late Early Triassic to the Middle Triassic, a major regression caused by early Indosinian movements occurred across the basin, resulting in the deposition of anhydrite, halite, and gypsiferous dolomite (Kang et al., 2000). Toward the end of the Middle Triassic, the rhomboid shape of the Sichuan Basin began to form as a result of compression from the Tethys Ocean plate to the southwest and the Pacific Ocean plate to the southeast. By the end of the Late Triassic, marine influence had diminished, and the basin became dominated by terrestrial deposits (Ma et al., 2007).

II.2 Depositional Environment and Sedimentary Facies

During the Permian, subsidence in the western part of studied area caused by growth faults led to the formation of a deep-water continental shelf (Figure 2.1B), whereas the

eastern part became a thick carbonate platform (Chen et al., 2014). With low amplitude sea level rise, biohermal facies such as reefs and shoals developed in margins of the rimmed carbonate platform. During the Early Triassic (Feixianguan Formation), after a wide-scale transgression and subsequent deposition of marginal carbonate shoal, the sea level decreased with basin uplifted, which led to the depositional environment changing from marginal carbonate platform to restricted platform landward. Lastly, due to decreasing water depths, an evaporitic platform capped with thick gypsum layer formed at the top of Feixianguan Formation, which also became the seal rock for the Feixianguan Formation reservoir (Ma et al., 2008).

Feixianguan Formation, deposited during the Early Triassic, is the main part of this carbonate platform. The facies changed from shallow marine open platform, platform margin, restricted platform to evaporitic platform landward (Ma et al., 2008; Sun et al., 2015). The main reservoir of the platform developed a marginal carbonate shoal with more than 150 m (490 ft) thick of ooid grains unit (Chen et al., 2014). The high hydrodynamic energy caused by storm waves provided a good environment for generation of ooid grains. After the diagenetic processes including dolomitization and dissolution enhanced pore space, sucrosic oolitic dolostone with great rock properties formed in the reservoir. However, compared with marginal carbonate shoals, restricted platform and open marine platform had relatively lower hydrodynamic energy and poorer reservoir quality.

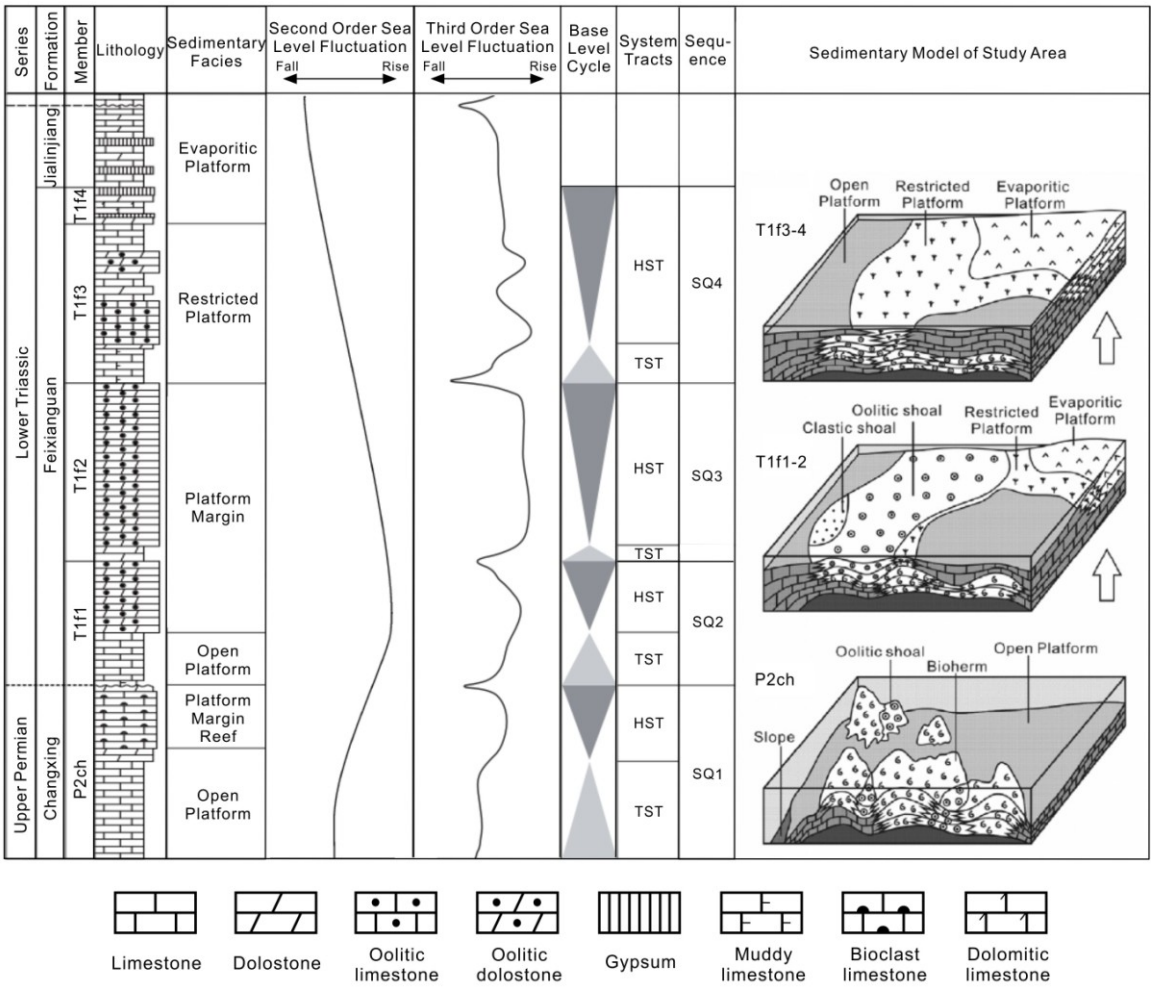

Figure 2.3: Stratigraphic column and depositional evolution from Permian to Triassic of the Sichuan Basin. (Modified from Yu et al., 2015, Sun et al., 2015 and Ma et al., 2008).

II.3 Sequence Stratigraphy

Feixianguan Formation can be sub-divided into four members: T1f1, T1f2, T1f3, and T1f4 from bottom to top (Ma et al., 2008; Sun et al., 2015). From the Late Permian to Early Triassic, a wide-range transgression happened in the beginning of T1f1 and followed a long regression until the end of T1f4. This 2nd-order sequence consists of three 3rd-order sequences, SQ2, SQ3 and SQ4, which is sub-divided by two unconformities at the top of T1f1 and T1f2 (Guo et al., 2012; Ma et al., 2008; Yu et al., 2015). T1f1 and

T1f2, formed by open platform marginal carbonate shoal deposits, consist of fine to medium oolitic dolomite and residual oolitic dolomite, with moldic and intercrystalline pore types, having good physical properties. T1f3 experienced the facies transition from restricted platform to evaporitic platform, corresponding to the rock type's change from dolomite to mudstone from base to top. T1f4 is composed of gypsum and shale deposited in an evaporitic platform (Ma et al., 2008). The Transgressive System Tract (TST) of each sequence is conductive to the form of limestone and oolitic dolostone with the syn-depositional diagenetic processes which includes cementation and micritization. The Highstand System Tract (HST) of each sequence provided a suitable environment for the generation of dolostone, which helps to enhance reservoir quality with dissolution and dolomitization.

II.4 Diagenesis

Diagenesis with different processes can produce special rock types and various pore structures (Figure 2.4). In the studied region, sediments experienced five stages of diagenesis from deposition to deep burial (Huang, 2017; Ma et al., 2008; Sun et al., 2015).

1) Syn-depositional marine cementation and micritization. Oolitic sediments experienced cementation and micritization in marine phreatic zone, with isopachous, fibrous, or micritic envelops around grains.

2) Meteoric dissolution and cementation. With sea level fall, the reef of Changxing Formation and oolitic shoal of Feixianguan Formation were exposed in the vadose zone

and selectively dissolved, which led to the development of intragranular and moldic pores with geopetal structures.

3) Dolomitization and cementation. After exposure to the atmosphere, these rocks were dolomitized in mixing water phreatic zone. Comparing with calcite, dolomite with lower solubility is favor to maintain primary pore and fracture.

4) Shallow burial diagenesis. During shallow burial, physical and chemical compaction and burial cementation reduced pore space, whereas dolomitization, recrystallization, and organic acid dissolution increased porosity and permeability.

5) Deep burial diagenesis. Due to the increase of burial depth and temperature, oil cracked into pyrobitumens and thermochemical sulphate reduction (TSR) occurred. The TSR reaction not only accelerated burial dolomitization, but also increased porosity by decreasing dolomite solubility and generating acid in pore waters.

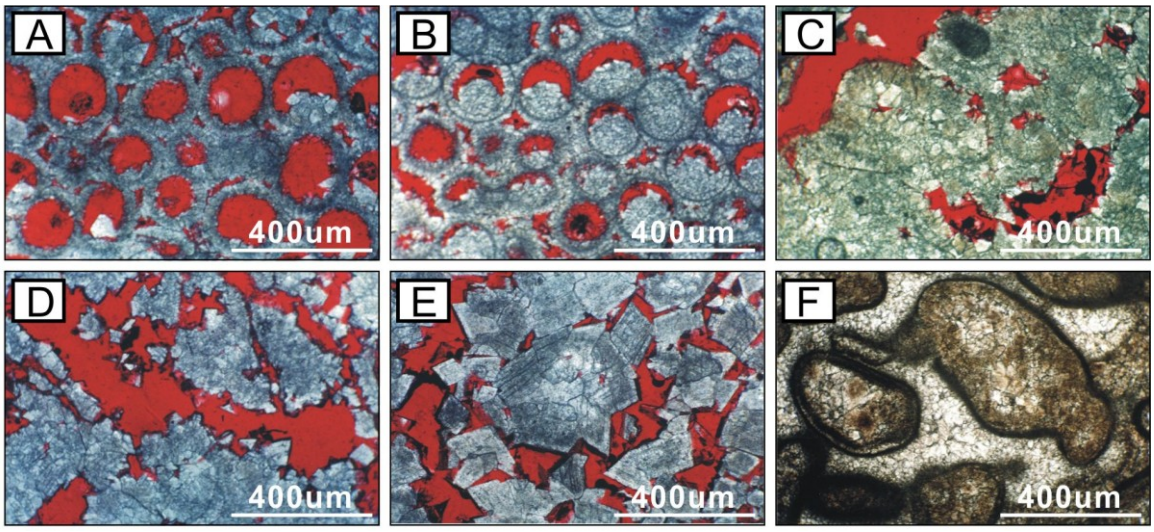

Figure 2.4: Different pore types observed in the thin sections with the same scale: A: moldic pores, B: moldic and intragranular pores, C: intragranular pores, D: intragranular and intercrystalline pores, E: intercrystalline pores, F: microcrystalline pores.

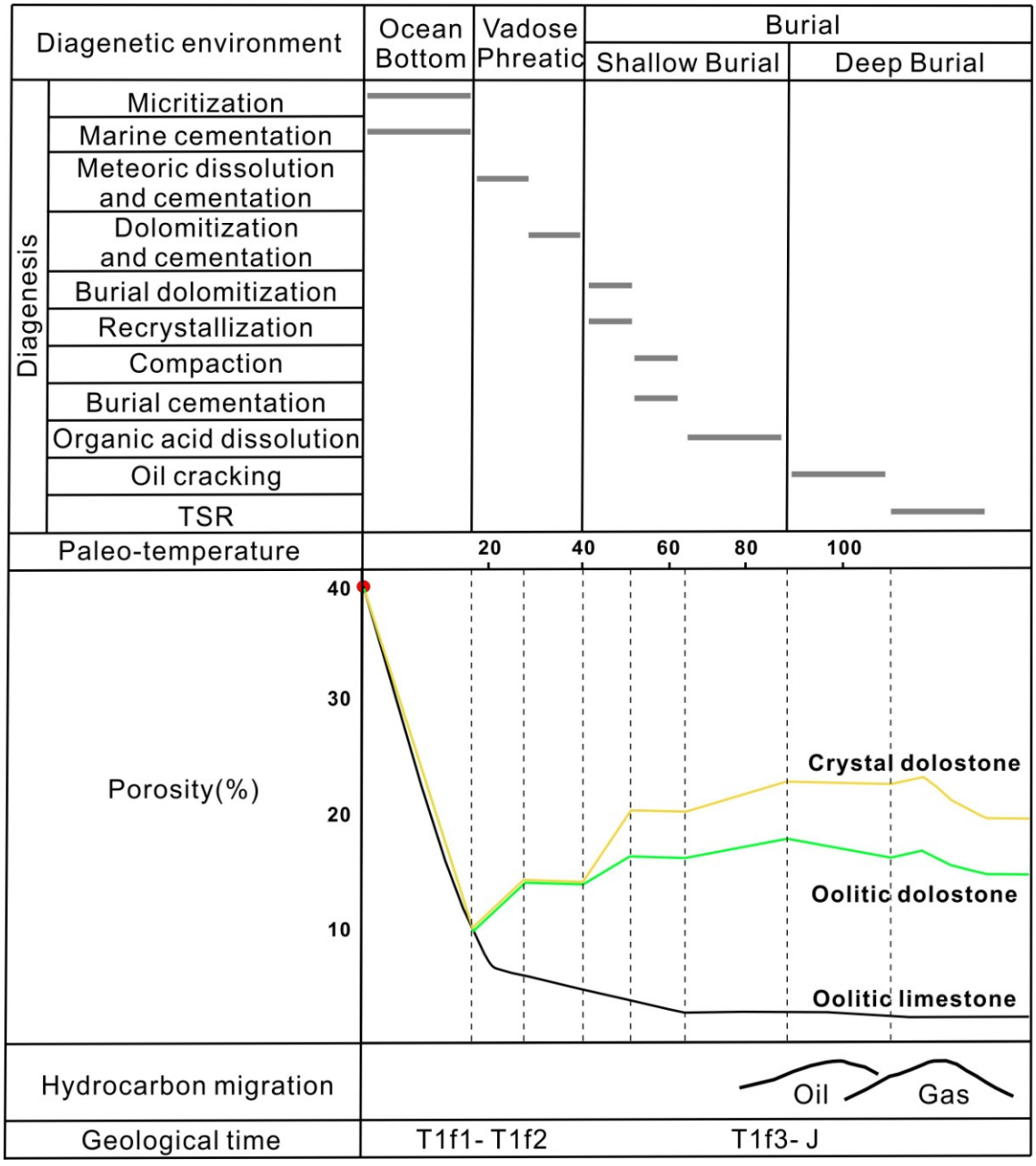

Figure 2.5: Paragenetic sequence and evolution of porosity in the Feixianguan Formation with the temperature in C^{o} (Modified from Sun et al., 2015 and Guo et al., 2012).

II.5 Reservoir Characterization

Diagenesis of the sediments in the depositional environment produced the Feixianguan Formation reservoirs consisting of oolitic dolostone, residual oolitic dolostone, crystalline dolostone and dolomudstone (Ma et al., 2008; Sun et al., 2015). Two main pore types occur in the reservoir: moldic pores and intercrystalline pores. A：Oolitic dolostone, developed in the oolitic shoal with moldic/intragranular pores, has high porosity but relatively low permeability. B: Residual oolitic dolostone possesses abundant mixed pores with high porosity and high permeability. C: Crystal dolostone consist of intercrystalline pores with low porosity but high permeability. These three described rock types developed in the edge of oolitic shoal. D: Dolomudstone is composed of fine dolomite crystals and microporous pores with low porosity and low permeability.

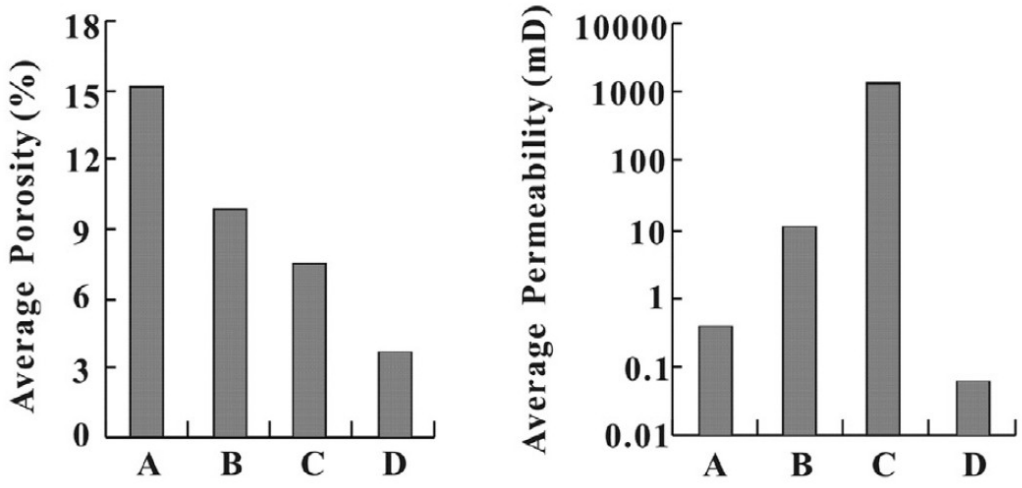

Figure 2.6: Reservoir porosity and permeability of different rocks in the Feixianguan Formations. A: oolitic dolostone, B: residual oolitic dolostone, C: crystal dolostone, D: dolomudstone (Modified from Sun et al., 2015).

CHAPTER III

ROCK PHYSICAL CHARACTERIZATION OF CARBONATE PORE STRUCTURES

III.1 Introduction

Carbonate rocks consist of assorted minerals and different pore structures as a result of varied depositional environments and subsequent diagenetic modification (Dunham, 1962; Lucia, 1995). The difference of pore types contributes to complicated relationships between porosity and permeability, which increases the difficulty of predicting permeability distribution. Therefore, a detailed study of pore structure is extremely critical for the estimation of rock properties, reservoir quality, and hydrocarbon recovery. Several carbonate rock pore type classification were established to distinguish various pore types based on the their genesis, geometries, and connectivity (Archie, 1952; Dunham, 1962; Lucia, 1995). With the analysis of core data, these classifications mainly come from petrographic and petrophysical observation and are used for pore type description with core or thin section available. However, a more accurate quantification is needed to classify pore structures with elastic parameters, which can be associated with well and seismic data. For example, the velocity-porosity model shows the effect of aspect ratio on scattered sonic log values (Xu and White, 1995). With aspect ratio increasing, the pore shape changes from linear to round leading to the increase of acoustic velocity. The modification of pore shape corresponds to the pore structure transformation from intercrystalline to moldic pores in the studied carbonate reservoir. A rock physics model was introduced to better estimate carbonate pore structure variation in a

quantitative method (Sun, 2000). In this model, the elastic parameters named frame flexibility factors (γ, γ_μ) can be used as the pore structure indicator, which reflect the difference of velocity caused by various pore types.

In Puguang Gas Field, due to the diversification of depositional facies and diagenetic process, reservoir pore evolved to different types in the Early Triassic Feixianguan Formation. Integrated study of core and well log data is used to understand carbonate pore structures and rock properties. The frame flexibility factor (γ) is used to indicate distinct pore types and become the pore structure index to analyze the relationship between permeability and porosity in this carbonate reservoir.

III.2 Methods

A rock physical model, as an extension of the Biot theory of poroelasticity, introduced elastic parameters called frame flexibility factors (γ, γ_μ), which help to understand rock properties with a given fluid and mineralogy (Biot, 1962; Y.F. Sun, 2000). Compared with previous studies, these frame flexibility factors depend less on porosity and indicate good relationship between pore structure, pore connectivity, and grain size. In this study, frame flexibility factors (γ, γ_μ) are used to quantitatively analyze carbonate reservoir rock pore structure, including pore size and shape. Some equation simplified by Sun (2000) are as the followings:

$$V_{\mathrm{p}} = \sqrt{\frac{K+\frac{4}{3}\mu}{\rho}} \tag{3.1}$$

$$V_{\mathrm{s}} = \sqrt{\frac{\mu}{\rho}} \tag{3.2}$$

$$K_{\mathrm{d}} = K_{\mathrm{s}}(1-\phi)^{\gamma} \tag{3.5}$$

$$\mu_{\mathrm{d}} = \mu_{\mathrm{s}}(1-\phi)^{\gamma_{\mu}} \tag{3.6}$$

For the studied gas-saturated reservoir, we simply use

$$K = K_{\mathrm{d}}$$

and

$$\mu = \mu_{\mathrm{d}} \tag{3.7}$$

Where V_{p} and V_{s} are the *P-wave* and *S-wave* velocities, K and μ are the bulk and shear moduli for the rock, respectively. ρ is density; porosity (ϕ) is derived from density log. K_{d} and K_{s} are the dry frame and solid matrix bulk moduli; μ_{d} and μ_{s} are dry frame and solid matrix shear moduli, respectively. γ and γ_{μ} are the frame flexibility factors.

III.3 Results

In this study, the effect of carbonate pore structure on reservoir rock properties is estimated using core and well log measurements. A frame flexibility factor (γ) from Sun Model (2000) is used to quantify various pore types classified from thin section. The relationship between porosity and permeability classified γ will be studied to understand pore structure influence for permeability heterogeneity.

III.3.1 Pore-Structure Analysis

A complicated relationship between porosity and compressional velocity occurs in the studied area. As Figure 3.1 shown, a given porosity corresponds to a diverse range of velocity values. Meanwhile, frame flexibility factor (γ) is helpful to characterize this complex relationship by classifying different pore types. Compressional velocity is influenced by varied geological factors, including porosity, mineral compositions, fluid features, and pore structures (Dou, 2011; Shi et al., 1989). In the studied field, most limestone transferred to dolostone after several stages of diagenesis and the reservoir layers are gas saturated. Therefore, the major factor for velocity difference is pore structure at similar porosity. Three main pore types, moldic, intercrystalline, and microcrystalline, occur in thin section. Physically, intercrystalline pores have lower aspect ratio than moldic pores and thus they have a lower compressional velocity within the same porosity range. It is shown that when $\gamma < 4.5$, the dominant pore type is moldic; when $4.5 < \gamma < 5.5$, moldic and intercrystalline pores are mixed in the rock samples; when $5.5 < \gamma < 15$, intercrystalline is prevalent; when $\gamma > 15$, microcrystalline pores dominate.

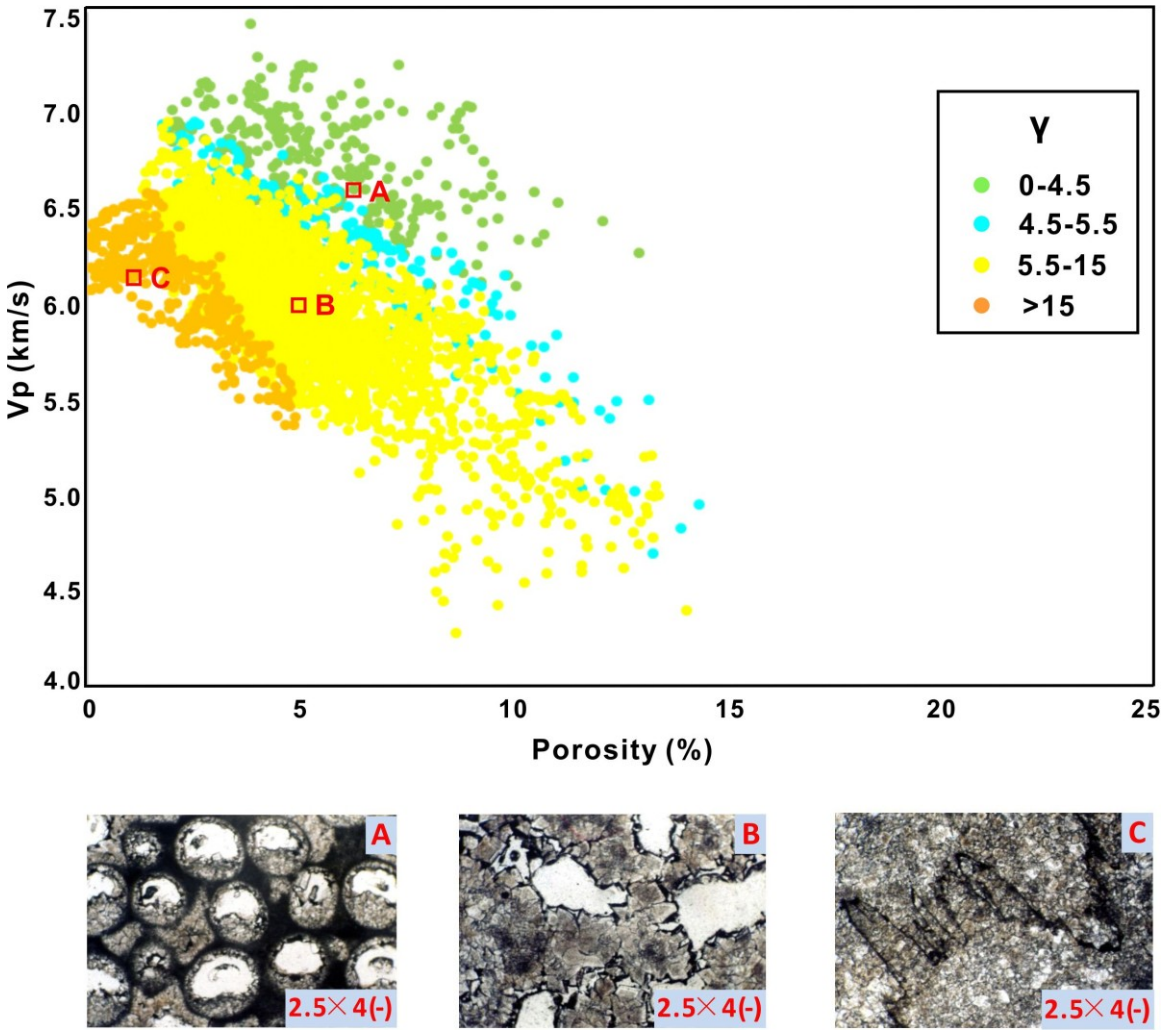

Figure 3.1: Cross-plot of compressional velocity Vp with density porosity. Frame flexibility factor γ is shown in color. Different pore types are shown in the thin section as following: A: moldic pores, B: intercrystalline pores, C: microcrystalline pores.

III.3.2 Permeability Estimation

Permeability heterogeneity, caused by pore structure variation, is extremely pervasive in carbonate reservoirs. Because of mineral sensitivity to depositional environment change such as porous fluid, temperature, and pressure, different pore types with similar porosity have exceedingly diverse permeability values. In this study, frame flexibility factor (γ) are used as an indicator of pore structures to classify the relationship between core porosity and core permeability, which both come from core sample laboratory measurements. Figure 3.2 shows two distinct porosity-permeability trends with different pore types. When $\gamma < 4.5$, the low permeability trend is observed in the ooid grainstone zone with isolated moldic pores. The porosity ranges between 0.01-0.29, and permeability ranges from 0.037-4.6 md. When $4.5 < \gamma < 5.5$, the reservoir rocks have mixed pore types, including both moldic and intercrystalline pores. When $5.5 < \gamma < 15$, the high permeability trend is observed in secondary intercrystalline pores. The porosity ranges between 0.01-0.16, and permeability ranges from 0.062-700 md. Within the high permeability trend, porosity and permeability increase with the development of dolomitization. Besides, when $\gamma > 15$, the microcrystalline pores that occur in dolomudstone retain small pore space and thus obtain some permeability, even in the lower porosity and permeability range.

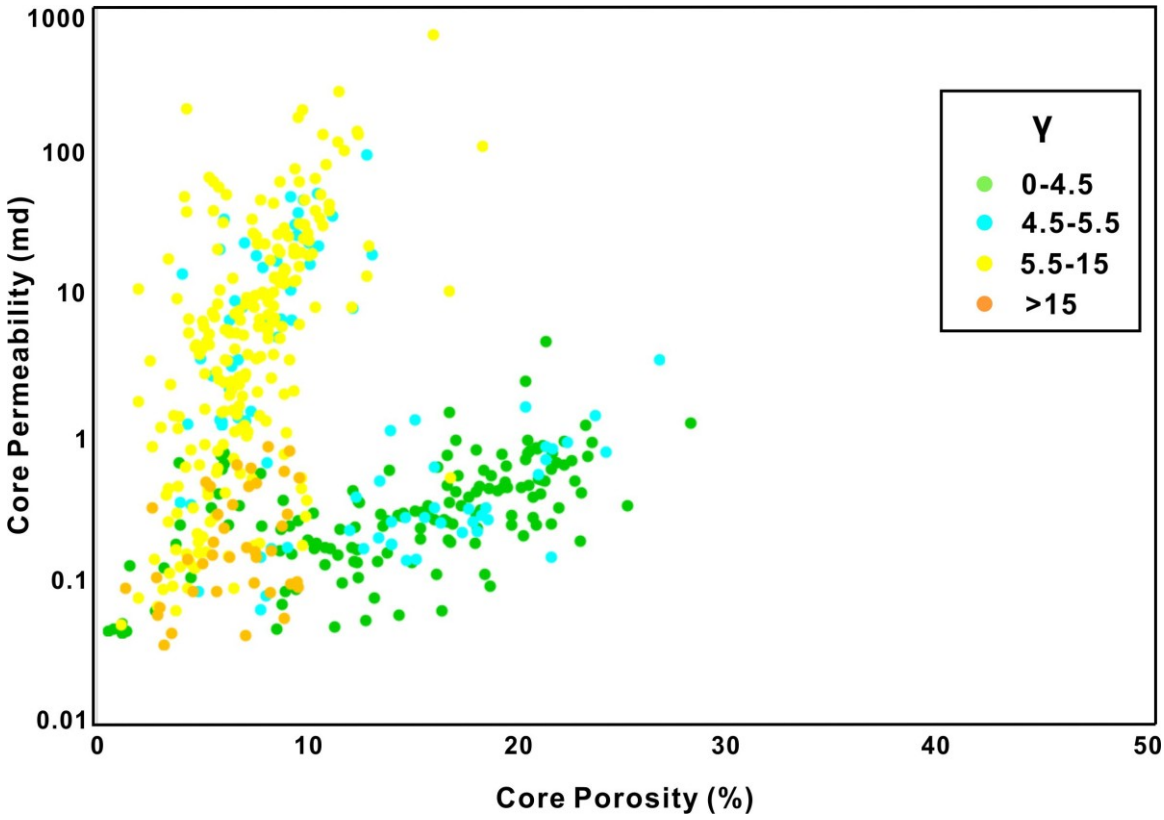

Figure 3.2: Cross-plot of core permeability with core porosity. Frame flexibility factor γ is shown in color.

In Figure 3.3, the crossplot shows the relationship between core permeability and the product of porosity and frame flexibility factor (γ). Two similar trends are observed with the pore structure indicator (γ). In the lower interval, the dominant pore type is isolated moldic pores. In the upper interval, intercrystalline pore is prevalent. Comparing Figure 3.2 and Figure 3.3, after adding γ as a pore structure indicator to the relationship between permeability and porosity, two permeability trends have a tendency to converge into one line. This alteration reconfirms that permeability is not only influenced by porosity, but also related to pore structure.

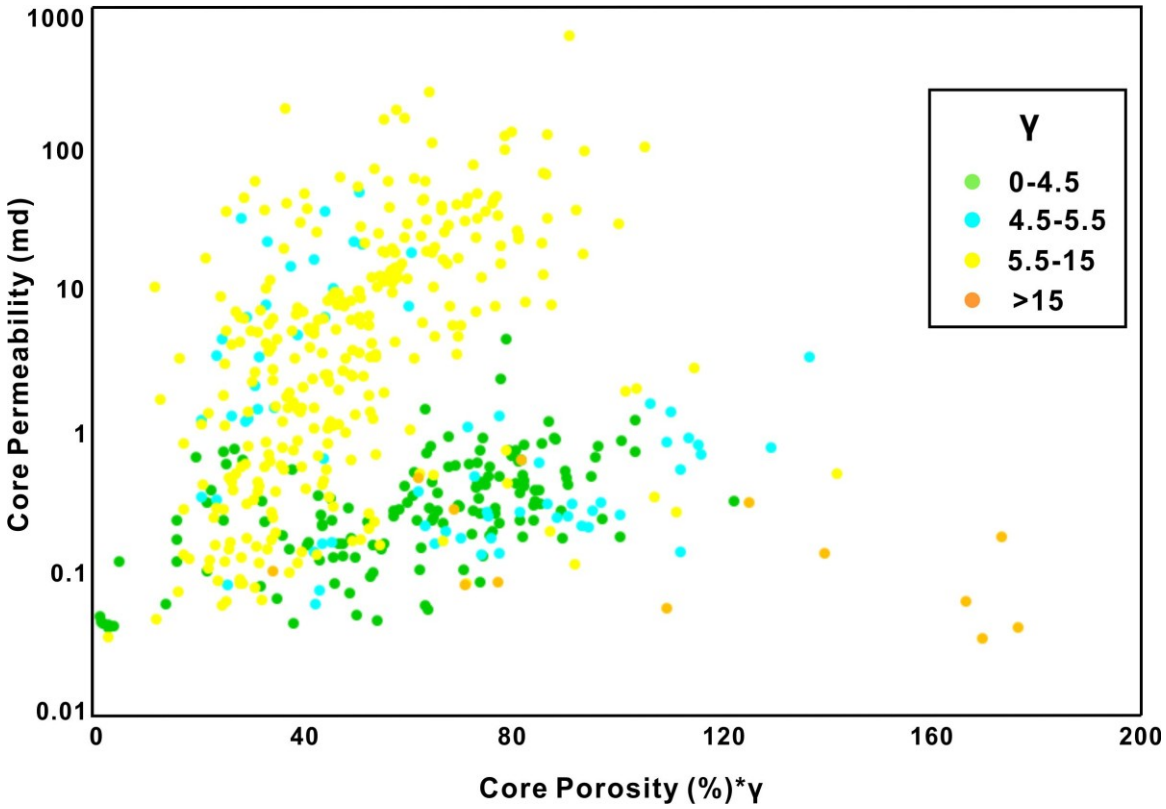

Figure 3.3: Cross-plot of core permeability with the product of core porosity and γ. Frame flexibility factor γ is shown in color.

Figure 3.4 shows a well-section of two cored wells in T1f1 and T1f2 formations. As the well correlation displays, frame flexibility factor γ is effective for distinguishing moldic and intercrystalline pores with a cut-off value of 5. Moldic and intercrytalline pores, both deposited in marginal carbonate shoals, have varied porosity-permeability relations due to different diagenesis. The moldic pores in ooid grains were created by partial dissolution after exposure, while intercrystalline pores were transformed from moldic during the process of reflux and burial dolomitization. The porosity and permeability data from lab measurements show that isolated moldic pores with good porosity have ordinarily high permeability values, whereas, well-connected

intercrystalline pores with even lower porosity may have extremely high permeability values.

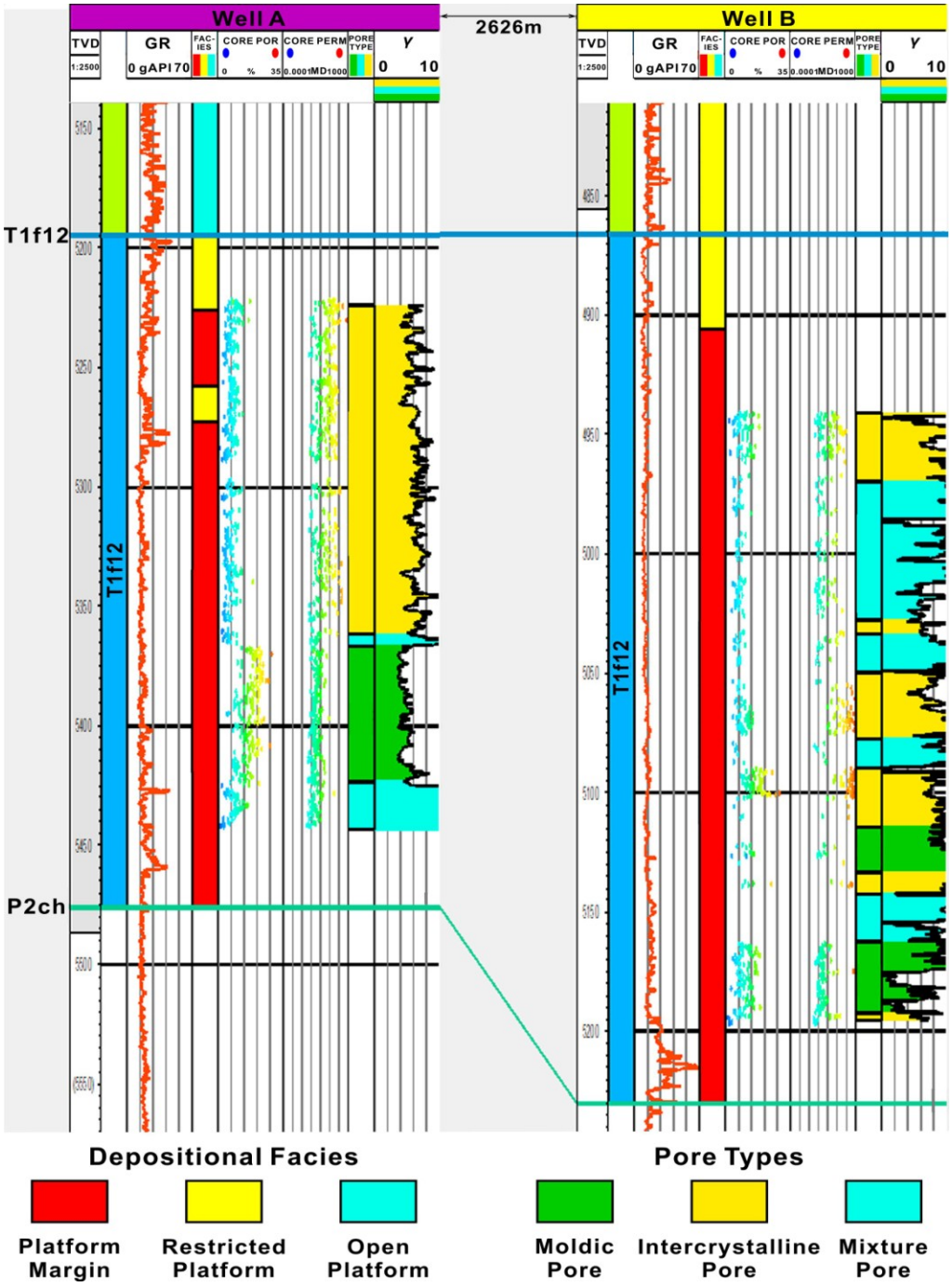

Figure 3.4: Well section of GR, depositional facies, core porosity, core permeability, frame flexibility factor γ, and pore structures. The location of well A and well B is shown in Figure 2.1.

III.4 Conclusions

The integrated study of core and log data can be used to estimate carbonate reservoir rock pore structures and predict spatial permeability heterogeneity. Three main pore types, moldic, intercrystalline, and microcrystalline pores, occur in thin sections in the Early Triassic reservoir in Puguang Gas Field. A frame flexibility factor (γ) shows a good relation with different pore shapes becoming the pore structure indicator in this study. When $\gamma < 4.5$, the dominant pore type is moldic; when $4.5 < \gamma < 5.5$, the mixture of moldic and intercrystalline pores occurs; when $5.5 < \gamma < 15$, intercrystalline is prevalent; when $\gamma > 15$, microcrystalline pores form. Because of the two distinct dominant pore types, two permeability-porosity trends exist classified by γ as a pore type index. In the lower permeability trend, the dominant pore type is moldic pores mainly formed in ooid grainstone. In the higher permeability trend, secondary intercrystalline pores are abundant. Compared to isolated moldic pores in ooid grains, dolomite crystals with well-connected pores have higher permeability in the same porosity range. Considering both porosity and pore types as influences of permeability, a better relationship among porosity, pore structures, and permeability is established.

CHAPTER IV

POST-STACK SEISMIC INVERSION AND RESERVOIR PERMEABILITY HETEROGENEITY ESTIMATION

IV.1 Introduction

Carbonate rock, containing diverse pore structures with various acoustic properties after diagenetic alteration, have complicated porosity and permeability relations. Therefore, acoustic information from well logs and seismic data can be used to estimate the variation of pore type and permeability. Many methods were developed to establish the correlation between pore shape and velocity. A frame flexibility factor (γ) from Sun model (2000) is used as a pore structure index to analyze the variation of elastic properties. This factor is effective for illustrating the velocity difference caused by pore type changes at a constant porosity and depends less on porosity (Sun, 2004). The method worked well in San Andreas Formation in Permian Basin, USA (Dou, 2011) and Bohai Bay Basin, China (Zhang, 2014) for the estimation of carbonate reservoir pore structure variation.

Different rocks with unique petrophysical properties such as rock fabric, grain size, and pore structure have diverse acoustic characteristics and thus can be distinguished in seismic data. A model-based seismic inversion method was introduced by Hampson and Russell (1991) to combine well log and seismic data together and improve the quality of inverted results. In post-stack inversion, acoustic impedance with lithology and fluid

information was derived from seismic data and is significant for interpretation of stratigraphic architecture and reservoir properties.

In the studied region, Early Triassic carbonate reservoirs experienced several sea level changes and varied diagenetic processes, which lead to different pore structures and strong permeability heterogeneity. We integrate core and log to analyze the variation of pore structures and its influence on acoustic properties with frame flexibility factor (γ) as a pore type indicator. Model-based acoustic impedance inversion using post-stack data is interpreted with rock petrophysical features to better understand the geological controls between pore structure and permeability heterogeneity.

IV.2 Methods

We applied frame flexibility factor (γ) from Sun (2000) model to indicate pore structure variation and evaluate permeability heterogeneity. We applied model based post-stack inversion to interpret acoustic impedance in order to understand different rock properties in studied carbonate reservoir.

IV.2.1 Rock Physics Model

We use the frame flexibility factor (γ) as an indicator to reflect the difference pore structures in gas-saturated carbonate reservoir. Based on the extension of the Biot theory of poroelasticity, Sun (2000) introduced a frame flexibility factor (γ) to analyze the effect of pore types on seismic velocity. The derivation of this factor is shown in Eqs.3.1-3.7 in Chapter III. In previous studies, γ is used to index various pore types and classify distinct

permeability trends in two different pore groups, namely, dominantly moldic and intercrystalline pores. Because γ is calculated from bulk moduli, we studied the relationship among γ, porosity, and P-wave velocity as well as acoustic impedance.

IV.2.2 Acoustic Impedance Inversion

In this study, model based post-stack inversion is applied to predict Acoustic Impedance (AI). Hampson and Russell (1991) proposed a model-based inversion method to improve seismic inversion quality. First, a geological model will be built from the well log and horizons interpreted from seismic data. Then, this stratal model will be compared with real seismic data. After these processes, the final inversion will match both well logs and seismic data. In term of seismic data type, the post-stack inversion will be performed and AI data volume will be generated in this study. AI inversion is a method to extract acoustic impedance from compressional velocity. AI can be used to understand rock elastic properties and has a linear correlation with the product of frame flexibility factor and porosity (Zhang, 2014).

IV.3 Results

In this study, the effect of carbonate pore structure on Acoustic Impedance (AI) variation and reservoir permeability heterogeneity is estimated using core, log, and seismic data. A frame flexibility factor (γ) from Sun Model is used to index pore types and analyze the geological control on well log and seismic data. The relationship between P-wave velocity and the product of porosity and γ as well as AI and the product are

established to further infer the spatial distribution of carbonate pore structures and high permeability zones.

IV.3.1 Pore-Structure Analysis

Pore structure variation has a great influence on acoustic velocities and elastic properties for carbonate rocks. Figure 4.1.a is a cross-plot of P-wave velocity versus density porosity with different pore structures classified by frame flexibility factor (γ). Verification by thin sections show that when the dominant pore type is moldic, the carbonate rock has a higher P-wave velocity with lower γ value; when the pore type is mixed by moldic and intercrystalline pores, the carbonate rock has a relatively high P-wave velocity with low γ value; when the dominant pore type is intercrystalline, the carbonate rock has a lower P-wave velocity with higher γ value; when the dominant pore type is microcrystalline, the carbonate rock has a lowest P-wave velocity with highest γ value.

In contrast to Figure 4.1.a, Figure 4.1.b shows the cross-plot of P-wave velocity versus the product of density porosity and γ with a more linear correlation. The relationship between P-wave velocity and the product of frame flexibility factor and porosity is

$$V_{\mathrm{p}} = A - B \times \phi\gamma \tag{4.1}$$

Where A and B are 7.021 and 0.023, respectively for the studied carbonate reservoir. R^2 is 0.8652.

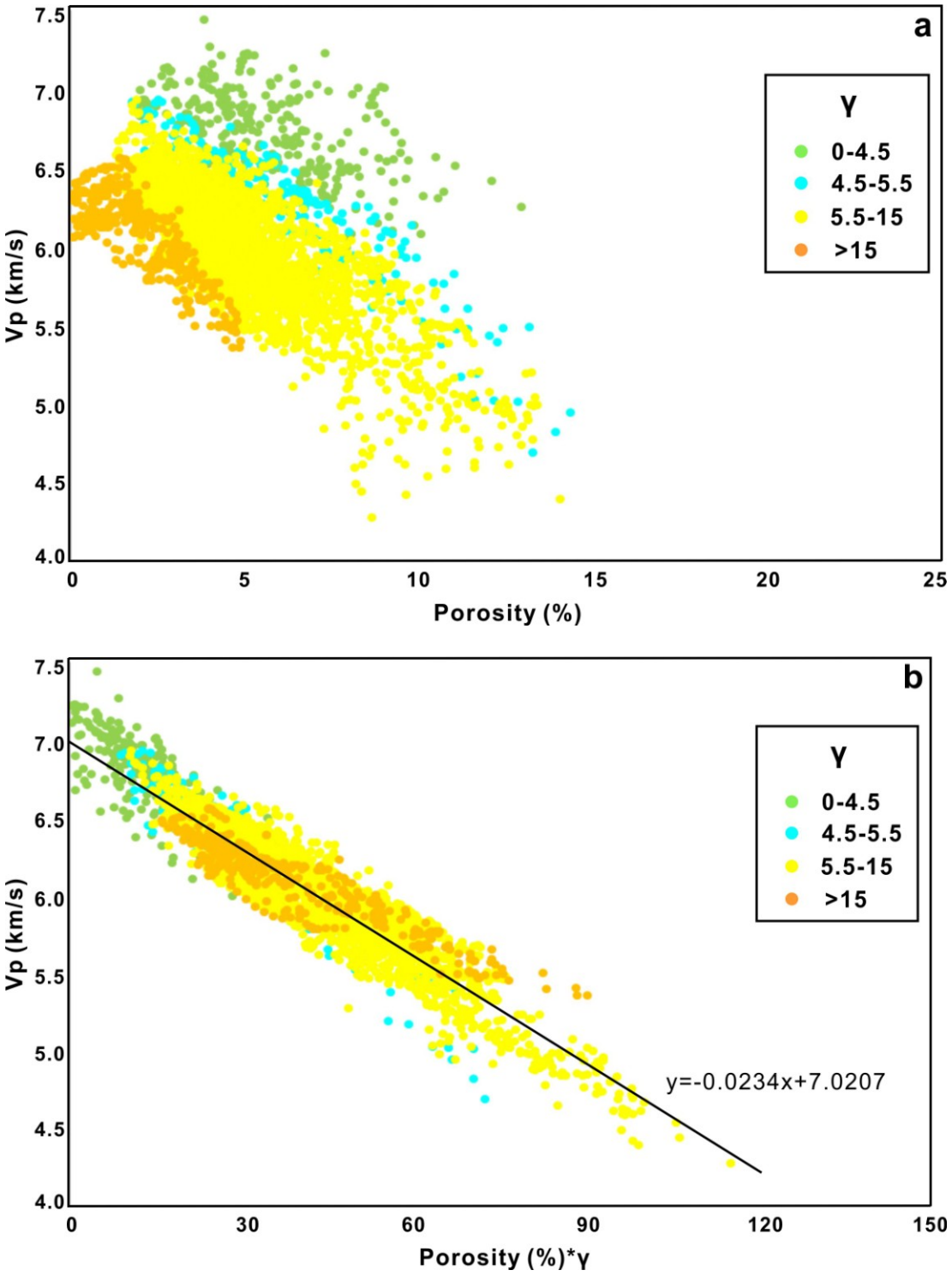

Figure 4.1: a) Cross-plot of P-wave velocity with density porosity. Frame flexibility factor γ is shown in color. **b)** Cross-plot of P-wave velocity with the product of density porosity and γ. Frame flexibility factor γ is shown in color.

As shown by Figure 4.2.a, acoustic impedance (AI) also is affected by pore types, represented by γ. When $\gamma < 4.5$, the dominant pore type is moldic and AI is highest; when $4.5 < \gamma < 5.5$, both moldic and intercrystalline pores occur and AI is relatively high; when $5.5 < \gamma < 15$, intercrystalline is prevalent and AI is lower; when $\gamma > 15$, microcrystalline pores form with lowest AI.

In order to better understand the effect of pore type variation on AI, we plot AI against the product of porosity and γ in Figure 4.2.b. After considering the influence of pore structure, the correlation is markedly over AI and porosity alone. In the upper part, isolated moldic pores are the main pore type; whereas in the lower part, well-connected intercrystalline pores dominate, since the intercrystalline pores have higher γ value than moldic pores when the porosity is similar. Therefore, at a given porosity, the intercrystalline pores with higher permeability have lower AI, whereas the moldic pores with lower permeability have relatively higher AI. The relationship between AI and the product of porosity and γ is

$$AI = C - D \times \phi\gamma \tag{4.2}$$

Where C and D are 19.567 and 0.082, respectively for the studied carbonate reservoir. R^2 is 0.8715.

Comparing Figure 4.2.b and 4.1.b, the correlation of AI and the product of porosity and γ is better than the correlation of P-wave velocity and the product of porosity and γ due to the impact of density. The AI variation with different pore structures can be useful for later AI inversion interpretation and reservoir permeability estimation.

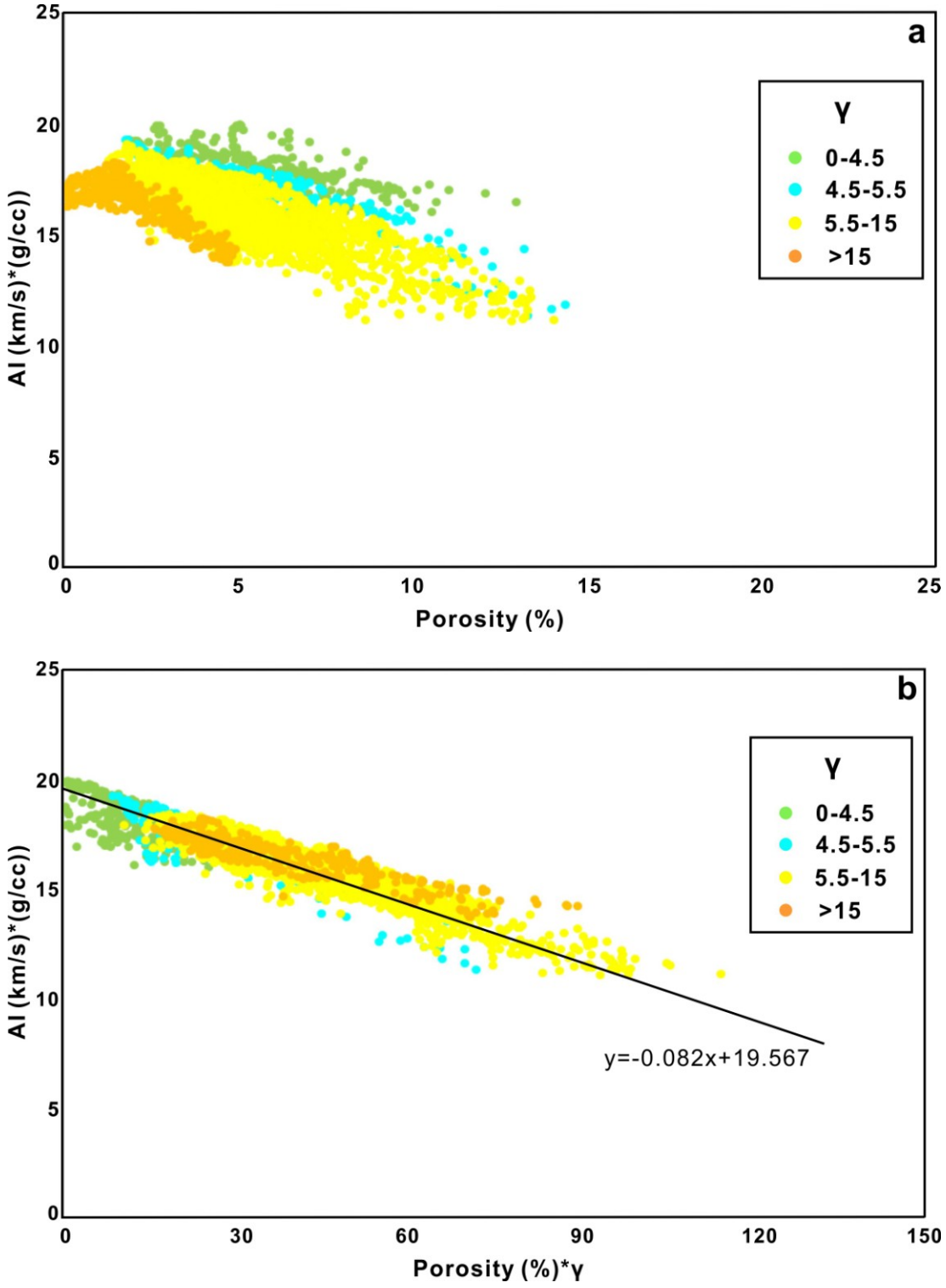

Figure 4.2: a) Cross-plot of AI with density porosity. Frame flexibility factor γ is shown in color. **b)** Cross-plot of AI with the product of density porosity and γ. Frame flexibility factor γ is shown in color.

IV.3.2 Post-Stack Acoustic Impedance Inversion

Acoustic impedance (AI), influenced by both velocity and density, plays a significant role on analysis of reservoir rock properties and stratigraphy. Figure 4.3 is a synthetic for well 3 using a zero-phase/100 ms wavelet. The correlation between the synthetic and a real seismic trace is 0.6. Three main reflection interfaces revealed by strong peak reflection can be traced in both synthetic and seismic data, marking the change of lithology around the bottom of T1f1, T1f3 and T1f4.

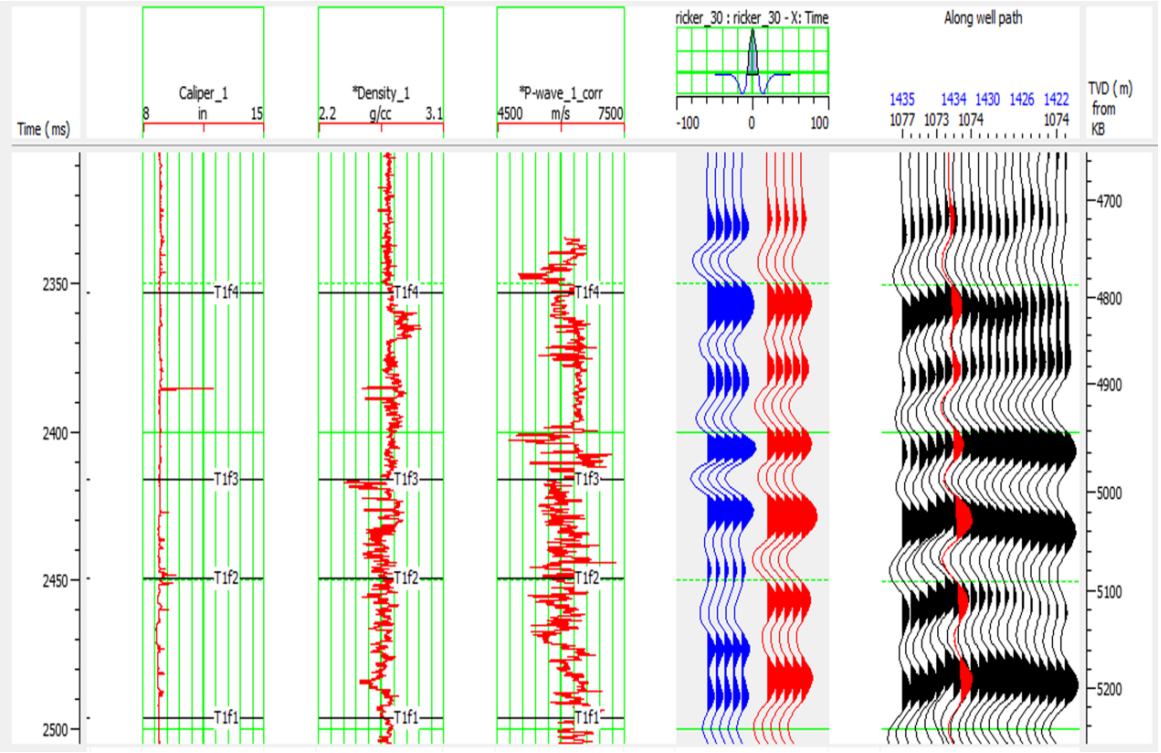

Figure 4.3: Seismic Well Tie for Well 3. The blue wiggle is the synthetic from well and the red wiggle is seismic trace.

Figure 4.4 shows one cross-section of three cored wells. The well correlations based on GR logs and cores agree with the previous studies from the core, log and seismic data in the following ways. From T1f1 to T1f4, ooid shoals were widely distributed in platform margin during the early regression. With the second-order sea level change, the depositional facies changed to restricted platform and finally replaced by evaporitic facies that developed at late regression. Consistent with the well correlation, the stratal model (Figure 4.5) displays a similar stratigraphy. In Early Triassic, the decrease of AI corresponds to the depositional environment changed from open platform to platform margin caused by a widely distributed transgression. A thick lower AI layer exists in T1f12 formation, which indicates ooid shoal deposited in platform margin in early regression. With continuous sea level reduce, the restricted platform occurred and following evaporitic platform with the development of gypsum layers, this alteration leads to the increase of AI value.

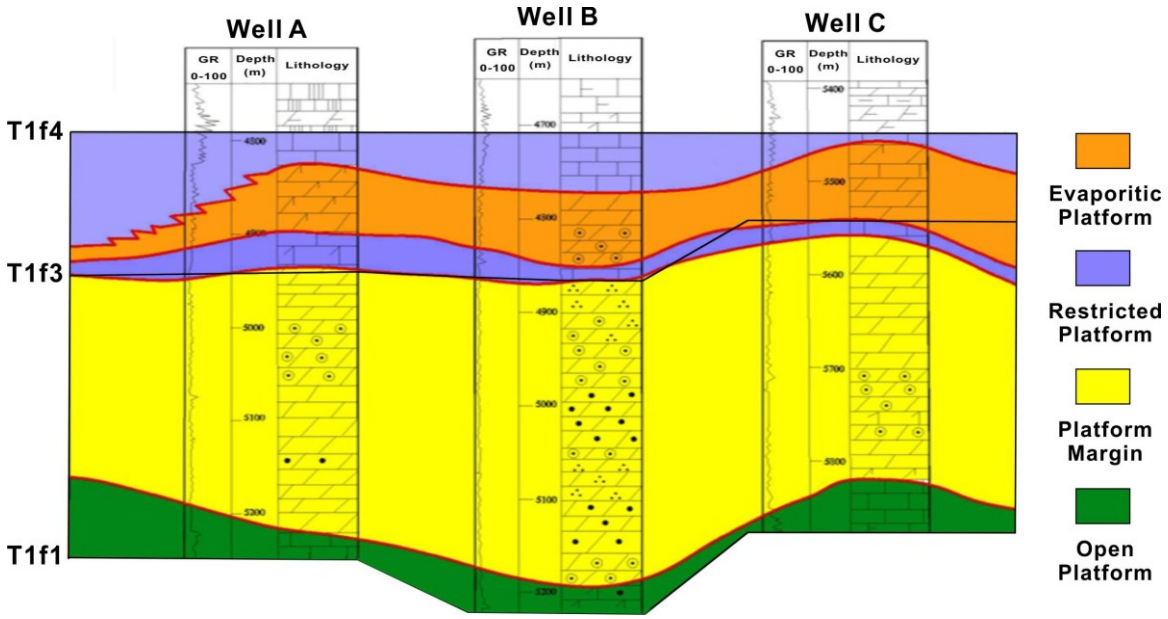

Figure 4.4: The well cross section of three wells with interpreted stratigraphic surfaces and depositional facies from the core and log analysis. The displayed log is GR. The line location is shown as A-A' in Figure 2.1.

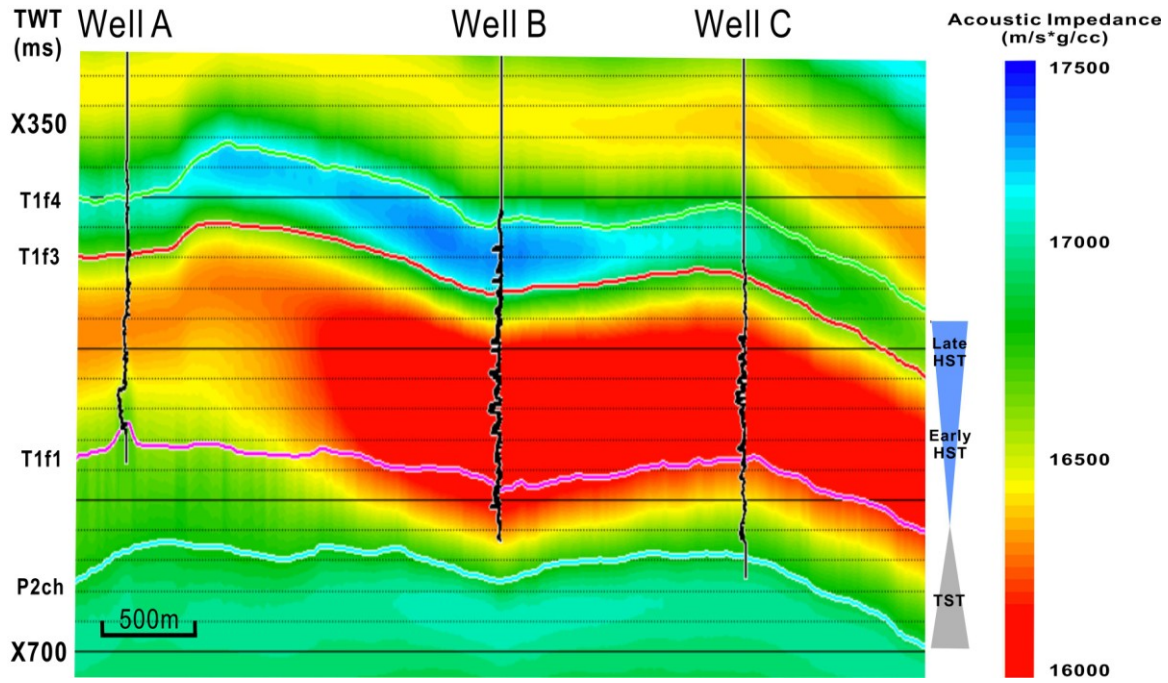

Figure 4.5: The stratal model built from acoustic impedance curves using the same three wells as shown in Figure 4.4. The line location is shown as A-A' in Figure 2.1.

Figure 4.6 shows five slices of AI extracted alone horizons P2ch, T1f1, T1f2, T1f3, and T1f4, respectively, in the studied area. Following the second-order sea level change, the Feixianguan Formation experienced a wide-spread transgression in the beginning of T1f1 followed by a long period regression until the end of T1f4. Slice 1 (P2ch) shows a wide distribution of high AI; slice 2 (T1f1) and slice 3 (T1f2) display the development of low AI; slice 4 (T1f3) and slice (T1f4) reveal the reduction of low AI and the extension of high AI.

The spatial variation of AI records varied rock properties caused by the change of depositional environment and sequence stratigraphy. In this studied region, A 2^{nd}-order sequence occurs and consists of three 3^{rd}-order sequences which are separated by two unconformities at the top of T1f1 and T1f2 (Guo et al., 2012; Ma et al., 2008; Yu et al., 2015). During the Early Triassic, a transgression favors the growth of ooid grains along platform margin with high hydrodynamics, following by a wide distribution of ooid shoals at the early regression. As sea level continued to fall, the water depth decreased in accommodation space in late regression, the depositional facies changed from a restricted platform to an evaporitic platform with the development of gypsum layers in the northeastern part of platform and open marine and lime mudstone in the southwest. The dolomitic ooid shoals with high porosity after diagenesis have low AI seismic response; whereas tight limestone and evaporitic dolostone and gypsum with low porosity result in high velocity, high density and high AI seismic responses.

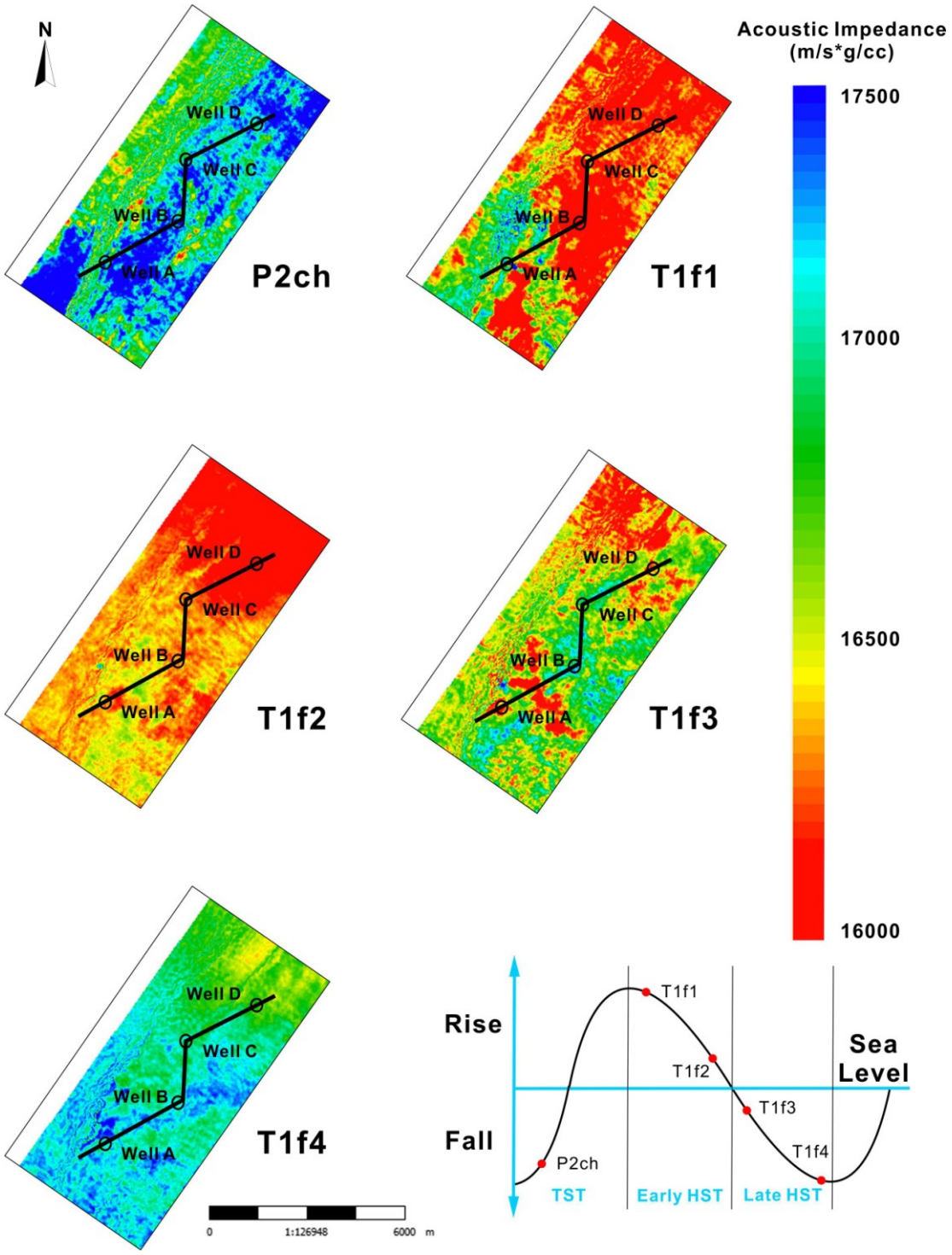

Figure 4.6: Five horizon slices of acoustic impedance volumes, parallel to the base of Feixianguan Formation, at different times following sea level fluctuation. The relative location of the slices on the 2nd-order sea level cycle is shown.

IV.3.3 Permeability Estimation

In carbonate reservoirs, permeability heterogeneity is essential for reservoir quality and can be strongly affected by different pore structures. In chapter III, two distinct permeability-porosity trends are classified by various pore type zones based on the pore structure indicator γ. As shown in Figure 3.2, when $\gamma < 4.5$, the low permeability trend is occurred in the ooid grainstone zone with isolated moldic pores. The porosity ranges between 0.01-0.29, and permeability ranges from 0.037-4.6 md. When $5.5 < \gamma < 15$, the high permeability trend consists of partially dissolved intercrystalline pores. The porosity ranges between 0.01-0.16, and permeability ranges from 0.062-700 md. When $4.5 < \gamma < 5.5$, the mixture of moldic and intercrystalline pores is found in both the low and high trends caused by the various proportion of these two pore types. With increasing porosity values, the difference of permeability drastically enlarges in these two pore types because of the unique pore structures and pore connectivity.

As the relationship of AI and the product of density porosity and γ showed in Figure 4.2.b, AI is also influenced by varied pore types. In the upper part, isolated moldic pores with relatively higher AI values are the main pore type; whereas in the lower part, well-connected intercrystalline pores with lower AI values dominate. Therefore, the intercrystalline pores with higher permeability have lower AI, whereas the moldic pores with lower permeability have relatively higher AI.

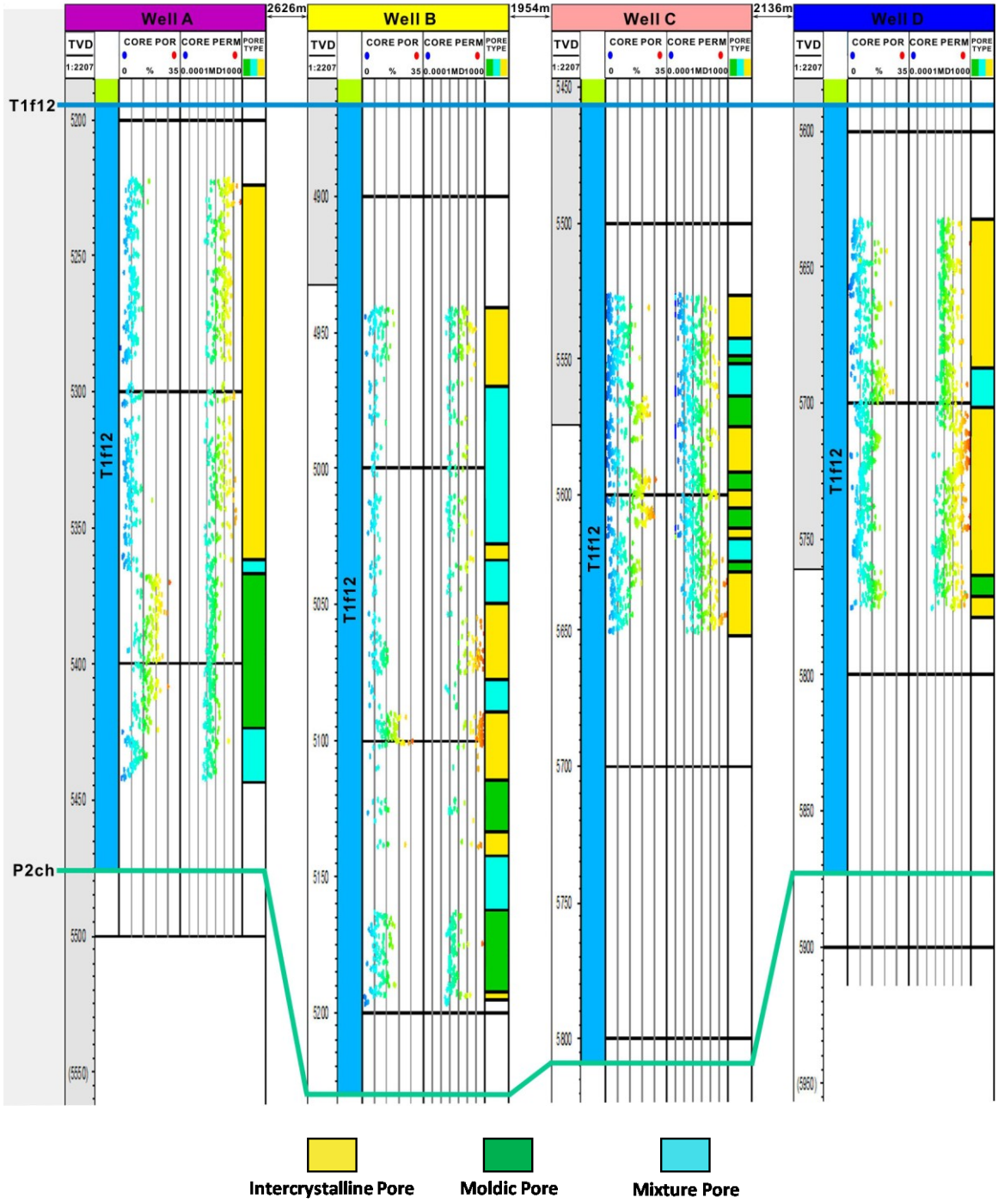

Figure 4.7: The well cross section of the same four wells is shown in Figure 4.5, with core porosity, core permeability, and pore types. The line location is shown as A-A' in Figure 2.1.

Figure 4.7 shows a well cross-section of four cored wells in T1f1 and T1f2 formations. The pore type is identified by thin section observation. As the well correlation displays, moldic and intercrytalline pores, both deposited in marginal carbonate shoal, have varied rock properties due to variable diagenetic histories and stratigraphic variations. From transgression to early HST, ooid shoals were widely developed on the platform margin, followed by the exposure in the late HST. The moldic pores in ooid grains were created and kept by partial dissolution and refluxion after exposure, whereas intercrystalline pores were transformed from moldic pores during the process of reflux and burial dolomitization. The core porosity and permeability log show that isolated moldic pores with good porosity have ordinarily high permeability values, whereas, well-connected intercrystalline pores with even lower porosity may have extremely high permeability values.

Compared with the well section, AI inversion (Figure 4.8) shows the similar result of the spatial distribution of various pore structures and permeability heterogeneity. In T1f1 and T1f2 formations deposited on platform margin shoals, the high AI beds, shown by green color, indicate moldic pore zones, which experienced partial dissolution and refluxion after exposure with relatively lower permeability values; the low AI beds, shown by yellow color, reflect the distribution of intercrystalline pores after reflux and burial dolomitization with relatively high permeability.

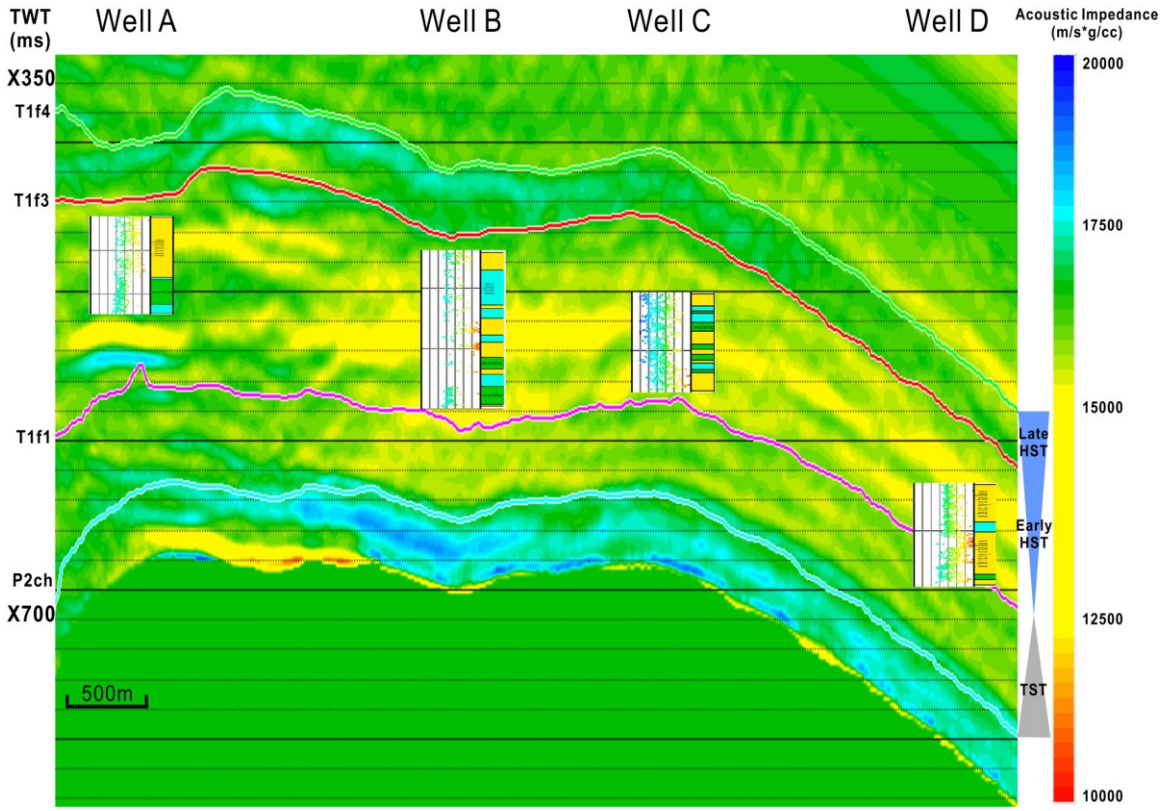

Figure 4.8: Post-stack acoustic impedance inversion result across four production wells with horizon interpretation illustrated. The inserted curves show measured core permeability and pore types. The line location is shown in Figure 2.1 as A-A'.

Figure 4.9 displays three RMS slices from TST, Early HST, and Late HST on the 2nd-order sea level cycle, indicating the spatial variation of permeability in different pore structures. Slices 1 shows a change from lime mudstone and dolostone with microcrystalline to a wide range of moldic pores formed in ooid shoals during transgression. Slice 2 illustrates the increasing of large intercrystalline pores occurred in platform margin in the early HST after further reflux and burial dolomitization. Finally, slice 3 reveals that moldic pores retained from burial dolomitization in restricted platform and microcrystalline pores formed in dolomudstone at late HST. The reservoir permeability increases with the transform of carbonate pore types from isolated moldic to

well-connected intercrystalline pores, and then decreases because of microcrystalline pores.

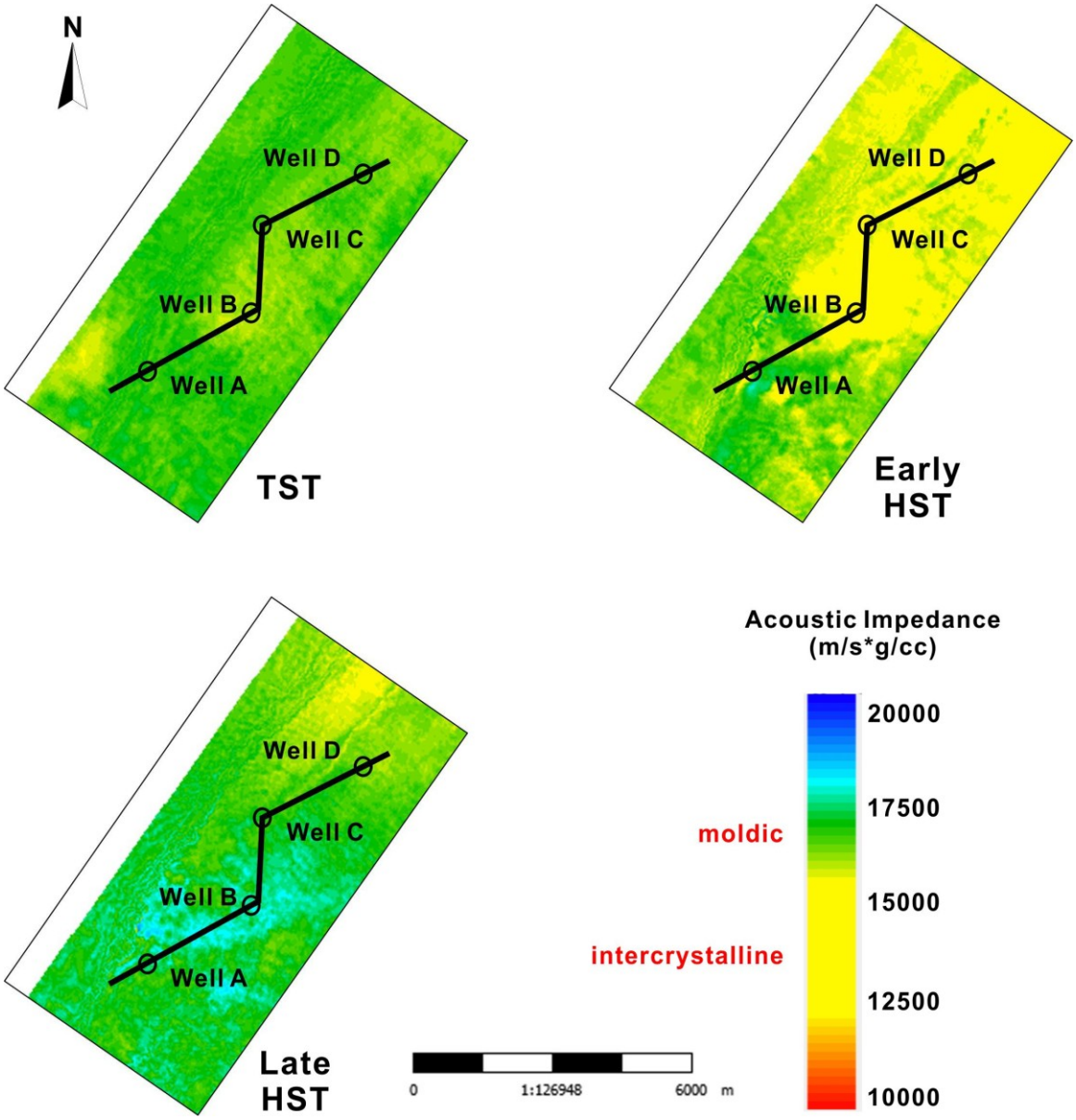

Figure 4.9: Three RMS slices of AI during TST, Early HST and Late HST on the 2nd order sea level cycle respectively. The change of color reflects spatial variation of permeability.

IV.4 Conclusions

Different carbonate pore structures created by geological changes such as sea level fluctuations, depositional facies and diagenesis can lead to the variation of elastic properties and porosity-permeability relationships. Frame flexibility factor (γ), as an index for varied pore shapes, can be used to analyze the impact of pore types on Acoustic Impedance (AI) and permeability.

The relationship between P-wave velocity and the product of porosity and γ as well as AI and the product are established. The latter correlation is better since AI is the function of velocity and density. In the upper part of the correlation of the correlation of AI and the product of porosity and γ, isolated moldic pores are the main pore type; while in the lower part, well-connected intercrystalline pores dominate, since the intercrystalline pores have higher γ value than moldic pores when the porosity is similar. These results from AI are used for further AI inversion interpretation.

Combined with the porosity-permeability relations consisting of two distinct trends associated with two main pore types, AI inversion can assist to quantify the spatial variation of pore structures and permeability. During the Early Triassic, a transgression favored the growth of ooid grains in platform margin with high hydrodynamics, following a wide distribution of ooid shoals with low AI at the early HST. After that, with the continuous decreasing of sea level in late HST, the depositional facies changed from restricted platform to evaporitic platform with the development of gypsum layers in the northeastern part of platform and open marine deposited lime mudstone in the southwest. The sediments in late HST with high velocity and density result in the high AI.

In carbonate margin shoal, moldic and intercrystalline pores developed after several diagenetic stages in T1f1 and T1f2 formation. Moldic pores created by partial dissolution after exposure have high AI seismic responding and relatively lower permeability value; whereas intercrystalline pores generated from reflux and burial dolomitization have low AI seismic responding to relatively higher permeability values.

CHAPTER V

SUMMARY

Carbonate rocks contain various pore structures as a result of geological influences including sea level changes, depositional environments, and diagenetic processes that complicate relationships between porosity and permeability. The Puguang Gas Field is a deeply-buried carbonate platform at a depth of about 5-6 km from the surface in Sichuan Basin, China. After deposition of platform margin shoals during transgression in Early Triassic, the main reservoir rock of the field experienced several diagenetic stages, such as meteoric dissolution, reflux and burial dolomitization, which lead to different pore structures, elastic properties, and even permeability heterogeneity.

Three main pore types, moldic, intercrystalline, and microcrystalline pores are observed from thin section in the Early Triassic reservoir. The frame flexibility factor (γ) calculated from Sun model shows a good relationship with different pore shapes becoming the pore structure indicator in this study. When $\gamma < 4.5$, the dominant pore type is moldic; when $4.5 < \gamma < 5.5$, the mixture of moldic and intercrystalline pores occurs; when $5.5 < \gamma < 15$, intercrystalline is prevalent; when $\gamma > 15$, microcrystalline pores form. Because of the two distinct dominant pore types, two permeability-porosity trends are classified by γ as a pore type indicator. In the lower permeability trend, the dominant pore type is moldic pores mainly formed in ooid grainstone. In the higher permeability trend, secondary intercrystalline pores are abundant. Compared to isolated moldic pores in ooid grains, dolomite crystals with well-connected pores have higher permeability in the same

porosity range. Considering both porosity and pore types as influences of permeability, a better relationship among porosity, pore structures, and permeability is established.

The relation between P-wave velocity and the product of porosity and γ as well as AI and the product are established. The latter correlation is better since AI is the function of velocity and density. In the upper part of the correlation of the correlation of AI and the product of porosity and γ, isolated moldic pores are the main pore type; while in the lower part, well-connected intercrystalline pores dominate, since the intercrystalline pores have higher γ value than moldic pores when the porosity is similar.

Combined with the porosity-permeability relations consisting of two distinct trends associated with two main pore types, AI inversion can assist to quantify the spatial variation of pore structures and permeability. During the Early Triassic, a transgression favored the growth of ooid grains in high hydrodynamics along platform margin, followed by a wide distribution of ooid shoals with low AI at the early HST. After that, with the continuously decreasing sea level in the late HST, the depositional facies changed from restricted platform to evaporitic platform with the development of gypsum layers in the northeastern part of platform and open marine deposited lime mudstone in the southwest. The sediments in late HST with high velocity and density result in the high AI. In carbonate margin shoals, moldic and intercrystalline pores developed after several diagenetic stages in T1f1 and T1f2 formation. Moldic pores were created by partial dissolution after exposure have high AI seismic response and relatively lower permeability values; whereas intercrystalline pores generated from reflux and burial dolomitization have low AI seismic response and relatively higher permeability values.

With the integrated study of core, log, and seismic data, the geological controls on pore structure variations play a critical role on permeability heterogeneity estimation and can improve the accuracy of reservoir prediction for further exploration.

REFERENCES

Biot, M. A. (1962). Mechanics of deformation and acoustic propagation in porous media. Journal of Applied Physics, 33(4), 1482–1498.

Cai, C., Xie, Z., Worden, R. H., Hu, G., Wang, L., & He, H. (2004). Methane-dominated thermochemical sulphate reduction in the Triassic Feixianguan Formation East Sichuan Basin, China: Towards prediction of fatal H2S concentrations. Marine and Petroleum Geology, 21(10), 1265–1279.

Chen, P. Y., Tan, X. C., Liu, H., Ma, T., Luo, B., Jiang, X. F., Jin, X. J. (2014). Formation mechanism of reservoir oolitic dolomite in Lower Triassic Feixianguan formation, northeastern Sichuan Basin, southwest China. Journal of Central South University, 21(8), 3263–3274.

Dou, Q. (2011). Rock physics-based carbonate reservoir pore type evaluation by combining geological, petro- physical and seismic data. Texas A&M University.

Dunham, R. J. (1962). Classification of Carbonate Rocks According to Depositional Textures. AAPG Memoir, 108–121.

G. E. Archie. (1952). Classification of Carbonate Reservoir Rocks and Petrophysical Considerations. AAPG Bulletin, 36(2), 278–298.

Guo, X. S.; Guo, T. L. (2012). The Exploration Theory and Practice of Large Gas Field in Puguang and Yuanba Carbonate Platform Margin (in Chinese).

Huang, Q. (2017). Geological Control on Permeability Heterogeneity in Deeply Buried Dolomite Rocks. Texas A&M University.

Kang, S. L., C. D. Fu, S. F. Cui, and X. Y. Y. (2000). Introduction to large- and medium-sized gas fields in China (in Chinese). Petroleum Industry Press, 328.

Lucia, F. J. (1995). Rock-Fabric / Petrophysical Classification of Carbonate Pore Space for Reservoir Characterization 1. AAPG Bulletin, 79(9), 1275–1300.

Ma, Y., Guo, X., Guo, T., Huang, R., Cai, X., & Li, G. (2007). The Puguang gas field: New giant discovery in the mature Sichuan Basin, southwest China. AAPG Bulletin, 91(5), 627–643.

Ma, Y. S., Guo, T. Lou, Zhao, X. F., & Cai, X. Y. (2008). The formation mechanism of high-quality dolomite reservoir in the deep of Puguang Gas Field. Science in China, Series D: Earth Sciences, 51(SUPPL. 1), 53–64.

Shi,Ge; Pan, R. (1989). The Application of seismic wave velocity determination to hydrocarbon exploration in carbonate-rock area. OGA, 24(6), 679–681.

Sun, P., Xu, H., Dou, Q., Adesokan, H., Sun, Y., Huang, Q., & Jiang, N. (2015). Investigation of pore-type heterogeneity and its inherent genetic mechanisms in deeply buried carbonate reservoirs based on some analytical methods of rock physics. Journal of Natural Gas Science and Engineering, 27, 385–398.

Sun, Y. F. (2000). Core-log-seismic integration in hemipelagic marine sediments on the eastern flank of the Juan de Fuca ridge. Proceedings of the Ocean Drilling Program, Scientific Results, Vol 168, 168, 21–35.

Sun, Y. F. (2004). Pore structure effects on elastic wave propagation in rocks: AVO modelling. Journal of Geophysics and Engineering, 1(4), 268–276.

Yu, Y., Tan, X., Chen, P., Yang, H., Ma, T., Cao, J., & Jin, X. (2015). Discovery of hiatus in Feixianguan Formation and its geological implications, Sichuan Basin, SW China. Turkish Journal of Earth Sciences, 24(1), 39–55.

Zhang, T. (2014). Integration of Rock Physics and Seismic Inversion for. Texas A&M University.

Zhang, X., Guo, T., Liu, B., Fu, X., & Wu, S. (2013). Porosity Formation and Evolution of the Deeply Buried Lower Triassic Feixianguan Formation, Puguang Gas Field, NE Sichuan Basin, China. Open Journal of Geology, 03(04), 300–312.